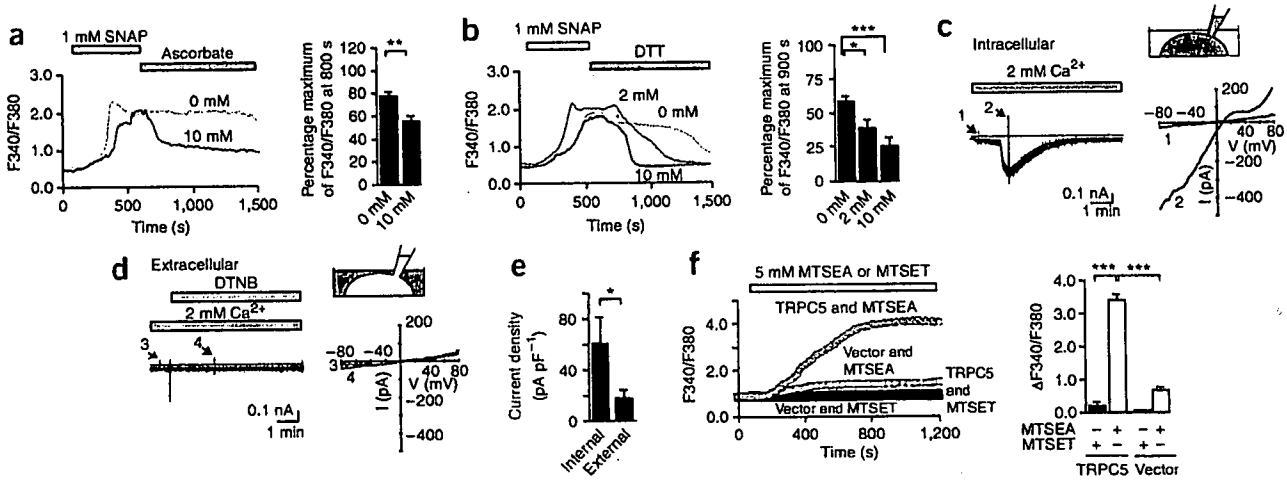

Figure 3 Chemical characterization and membrane sidedness of the action of NO and reactive disulfide in activating TRPC5 channels. (a,b) Ascorbate and DTT suppress TRPC5 responses to SNAP: representative time courses (left) and percentages of $[Ca^{2+}]_i$ rises (right) at 800 s (a) and 900 s (b) relative to maximal rises (n = 17–42). $^*P < 0.05$, $^{**}P < 0.01$ and $^{***}P < 0.001$. (c,d) Whole-cell TRPC5 currents are activated by DTNB (left) via internal dialysis (10 μM) (c) but not via external application (30 μM) (d). I–V relations were determined using 50-ms positive-voltage ramps from –80 mV to +80 mV applied at time points indicated as 1–4 (right). (e) Peak current densities (n = 22–27). $^*P < 0.05$. (f) Ca^{2+} responses to MTSEA or MTSET: average time courses (left) and maximal $[Ca^{2+}]_i$ rises (right) (n = 17–33). Data points are mean ± s.e.m. $^{***}P < 0.001$.

suggest that the group of native S-nitrosylation–sensitive TRP channels mediates a ubiquitous mechanism that is critical for feedback regulation of Ca^{2+} signals by NO.

RESULTS

NO activates TRPC5 channels via sulfhydryl modifications

Recombinant expression of TRPC5 elicited robust elevation of $[Ca^{2+}]_i$ in response to the NO donor *S*-nitroso-*N*-acetyl-DL-penicillamine (SNAP, **1**) in human embryonic kidney (HEK) cells (**Fig. 1**). A similar $[Ca^{2+}]_i$ increase was induced by another NO donor, (±)-(*E*)-4-ethyl-2-[(*E*)-hydroxyimino]-5-nitro-3-hexenamide (NOR3, **2**), but not by the peroxynitrite donor 3-(4-morpholinyl)sydnonimine hydrochloride (SIN-1, **3**) (**Fig. 1c**). The SNAP-induced Ca^{2+} response is attributable mainly to Ca^{2+} entry through the TRPC5 channel, as SNAP evoked only marginal $[Ca^{2+}]_i$ rises in TRPC5-expressing cells after omission of extracellular Ca^{2+} (**Supplementary Fig. 1** online) and in vector-transfected control cells (**Fig. 1a**). The sensitivity of TRPC5 to SNAP was prominent among TRPC homologs: substantial $[Ca^{2+}]_i$ rises distinguishable from the control were elicited by TRPC5 in response to SNAP at 10 μM, but such rises were elicited by TRPC3 and TRPC7 and by the redox status–sensitive Ca^{2+}-permeable cation channel TRPM2 (ref. 28) only at much higher concentrations of SNAP, such as 300 μM. TRPM2 mediated pronounced Ca^{2+} responses to H_2O_2 (**Fig. 1b**). TRPC5 was the only TRPC homolog that elicited robust Ca^{2+} responses to H_2O_2 at 100 μM (**Fig. 1b**). Furthermore, ATP/Mg^{2+}-sensitive Ca^{2+}-permeable cation channel TRPM7 (ref. 3), which responds to oxygen- and glucose-deprived conditions[29], was responsive to H_2O_2 but not to SNAP (**Fig. 1a,b**). Thus, prominent sensitivity to NO is characteristic of TRPC5 channels.

NO-induced Ca^{2+} responses mediated by TRPC5 were resistant to the guanylate cyclase inhibitor 1H-[1,2,4]oxadiazolo[4,3-a]quinoxalin-1-one (ODQ, **4**) (**Supplementary Fig. 1**). This suggests that NO acts through cGMP-independent pathways such as nitrosylation of free sulfhydryl groups of cysteine residues. Indeed, among reactive disulfides that selectively detect free sulfhydryl groups of cysteine residues in proteins (**Fig. 2a**), membrane-permeable pyridyldisulfides (PDS) such as 2,2′-dithiobis(5-nitropyridine) (5-nitro-2-PDS, **5**), 2,2′-dithiodipyridine (2-PDS, **6**) and 4,4′-dithiodipyridine (4-PDS, **7**) induced robust $[Ca^{2+}]_i$ rises in cells expressing TRPC5, whereas membrane-impermeable analog 5,5′-dithiobis(2-nitrobenzoic acid) (DTNB, **8**) elicited marginal $[Ca^{2+}]_i$ elevation that was indistinguishable from the control (**Fig. 2b,c**). Expression of other TRPCs and of TRPM2 and TRPM7 failed to elicit 5-nitro-2-PDS–induced $[Ca^{2+}]_i$ increases that significantly surpassed the control. TRPC5 responses to SNAP, 5-nitro-2-PDS and H_2O_2 were preceded by time lags after application (time to half peak was 305 ± 14.4 s for 300 μM SNAP (n = 52), 780 ± 50.1 s for 1 mM H_2O_2 (n = 18), and 425 ± 32.7 s for 30 μM 5-nitro-2-PDS (n = 17)). Robust TRPC5-mediated responses were evoked by simultaneous application of SNAP (30 μM) and 5-nitro-2-PDS (3 μM), which both induced slight TRPC5 responses when individually applied (**Fig. 2d**). Furthermore, maximal responses elicited by 1 mM SNAP were not potentiated by the addition of 30 μM 5-nitro-2-PDS, and vice versa (**Supplementary Fig. 2** online). These relationships may imply a common action site (or sites) for NO and 5-nitro-2-PDS in inducing TRPC5 responses. Thus, reactive disulfides are useful tools for identifying the free sulfhydryl targets of NO in TRPC5 activation.

The reducing agent ascorbate (**9**) significantly (P = 0.008) diminished SNAP-induced TRPC5 responses (**Fig. 3a**) but not 5-nitro-2-PDS–induced TRPC5 responses (**Supplementary Fig. 2**). Dithiothreitol (DTT, **10**) had a potent suppressive effect on both responses (**Fig. 3b** and **Supplementary Fig. 2**). Considering the reported selective reduction of nitrosothiol by ascorbate to reform thiol[10], this result supports the notion that NO and reactive disulfides form nitrosothiols and disulfide bonds, respectively, on cysteine residues in eliciting TRPC5-mediated responses. After washout, the TRPC5 response to SNAP was slowly attenuated (**Fig. 3a,b**), in contrast to the sustained TRPC5 response to 5-nitro-2-PDS (**Supplementary Fig. 2**). This suggests that the nitrosylation is reversed by intrinsic antioxidants in HEK cells. The modification stability, the TRPC5 selectivity and the substitutability for NO of reactive disulfides prompted us to use them as tools in the following studies on TRPC5 activation.

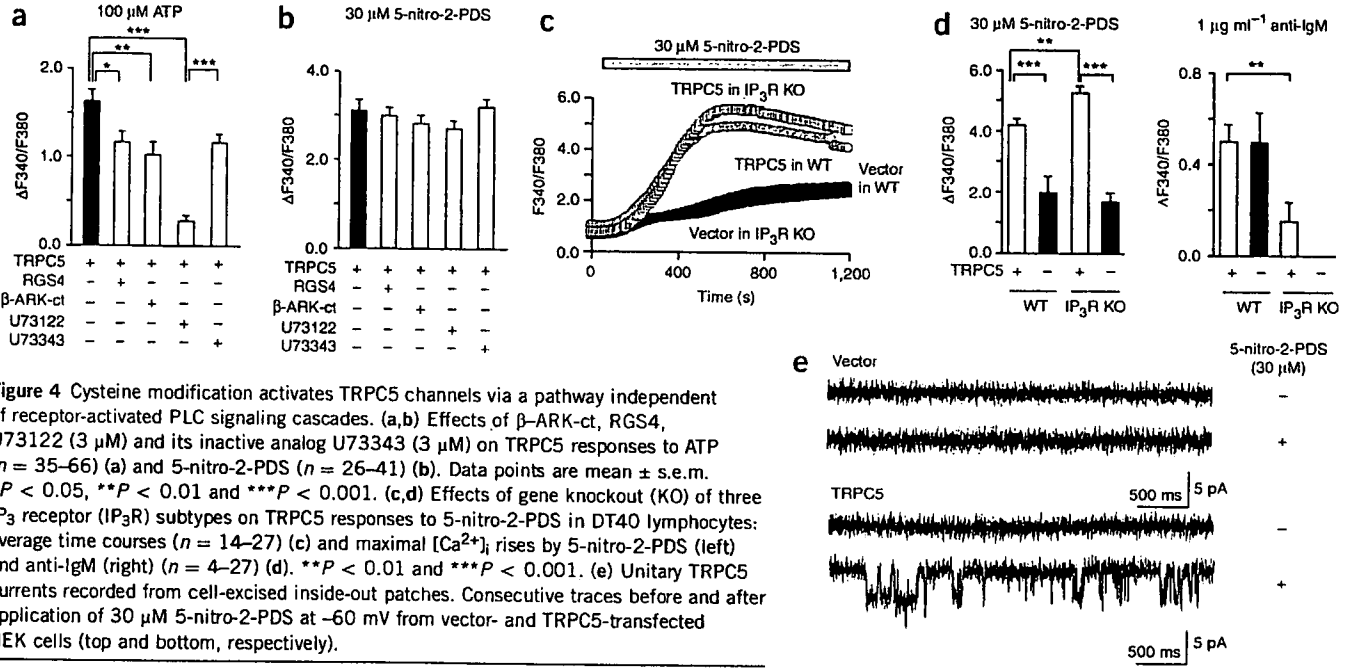

Figure 4 Cysteine modification activates TRPC5 channels via a pathway independent of receptor-activated PLC signaling cascades. (a,b) Effects of β-ARK-ct, RGS4, U73122 (3 μM) and its inactive analog U73343 (3 μM) on TRPC5 responses to ATP (n = 35–66) (a) and 5-nitro-2-PDS (n = 26–41) (b). Data points are mean ± s.e.m. $^*P < 0.05$, $^{**}P < 0.01$ and $^{***}P < 0.001$. (c,d) Effects of gene knockout (KO) of three IP_3 receptor (IP_3R) subtypes on TRPC5 responses to 5-nitro-2-PDS in DT40 lymphocytes: average time courses (n = 14–27) (c) and maximal $[Ca^{2+}]_i$ rises by 5-nitro-2-PDS (left) and anti-IgM (right) (n = 4–27) (d). $^{**}P < 0.01$ and $^{***}P < 0.001$. (e) Unitary TRPC5 currents recorded from cell-excised inside-out patches. Consecutive traces before and after application of 30 μM 5-nitro-2-PDS at −60 mV from vector- and TRPC5-transfected HEK cells (top and bottom, respectively).

In TRPC5-expressing cells, 5-nitro-2-PDS–induced Ca^{2+} responses are due to Ca^{2+} entry through the TRPC5 channel, as $[Ca^{2+}]_i$ elevation was evoked predominantly upon readdition of extracellular Ca^{2+} (**Supplementary Fig. 2**). The whole-cell mode of the patch clamp method demonstrated 5-nitro-2-PDS–induced inward currents that developed gradually in TRPC5-expressing cells (n = 6), but not in control cells (n = 4), at a holding potential (V_H) of −60 mV (**Supplementary Fig. 2**). Current–voltage (I–V) relationships of the 5-nitro-2-PDS–activated currents corresponded well with previously reported receptor-activated TRPC5 currents[30]. 5-nitro-2-PDS–activated TRPC5 currents showed a resistance to washout that was slowly reversed by DTT (n = 5), which supports $[Ca^{2+}]_i$ measurements.

Membrane sidedness of modification in TRPC5 activation

The ineffectiveness of extracellular application of the membrane-impermeable DTNB (**Fig. 2c**) suggests an agonistic modification site (or sites) that is accessible only from the cytoplasmic side. We explicitly evaluated this hypothesis using the patch clamp method. Intracellular perfusion of DTNB from the patch pipette elicited TRPC5 currents at a V_H of −60 mV with a time lag of 1 to 2 min after the whole-cell mode was established (**Fig. 3c**). The I–V relationship was similar to that activated by 5-nitro-2-PDS (see above). However, extracellular DTNB exerted no significant effects on current levels or I–V relationships in TRPC5-expressing cells (**Fig. 3d,e**). The action of methanethiosulfonate derivatives, which directly modify free cysteine thiols by forming a disulfide bond[31], resembled the action of reactive disulfides in sidedness: membrane-permeable 2-aminoethylmethanethiosulfonate hydrobromide (MTSEA, **11**) but not membrane-impermeable [2-(trimethylammonium)ethyl]methanethiosulfonate bromide (MTSET, **12**) induced TRPC5 responses via extracellular administration (**Fig. 3f**). These results support the cytoplasmic accessibility of the site for cysteine modifications.

Identification of the site of cysteine modification in TRPC5

We have previously demonstrated metabotropic ATP receptor subtype P2Y-mediated activation of TRPC5 channels via the G-protein isoform Gq and PLC-β in HEK cells[30]. Therefore, we examined the possibility that the P2Y-activated signaling cascade has an action site (or sites) for reactive disulfides in TRPC5 activation. The quenching of G protein βγ complexes by the regulator of G-protein signaling 4 (RGS4) (P = 0.011) and the C terminus of β-adrenergic receptor kinase (β-ARK-ct) (P = 0.002), as well as the inhibition of PLC-β by the PLC inhibitor U73122 ($P < 0.001$), significantly attenuated TRPC5 responses to P2Y stimulation but failed to affect TRPC5 responses evoked by 5-nitro-2-PDS (**Fig. 4a,b**). Furthermore, disruption of the three IP_3 receptor subtype genes[32], which suppressed IgM-induced TRPC5 responses via B-cell receptors, significantly promoted 5-nitro-2-PDS–evoked TRPC5 responses in DT40 B lymphocytes (**Fig. 4c,d**). These results suggest that reactive disulfides activate the TRPC5 channel independently of P2Y-activated signals.

We examined whether reactive disulfides directly act on TRPC5 channels using the cell-excised, inside-out mode of patch clamp recording. Single-channel currents with a unitary conductance of 44.1 pS were induced in TRPC5-expressing cells (but not in control cells) by applying 5-nitro-2-PDS to the cytoplasmic side of excised patches (**Fig. 4e**). On the basis of this result, we hypothesized that the action site is localized at the plasma membrane and its associated cellular components in TRPC5-expressing cells. Therefore, we investigated the incorporation of reactive disulfides into TRPC5 channel complexes using DTNB-2Bio (**13**), a DTNB derivative that has two biotin groups attached (**Fig. 5a**; **Supplementary Scheme 1** and **Supplementary Fig. 3** online). In cells expressing green fluorescent protein (GFP)-tagged TRPC5, we incorporated DTNB-2Bio into a ~130 kDa protein band, which yielded an adduct whose molecular weight corresponds well with the calculated molecular weight of TRPC5-GFP (139 kDa) (**Fig. 5b**). Simultaneous application of SNAP inhibited the incorporation of DTNB-2Bio (**Fig. 5c**), which is consistent with the observation in the $[Ca^{2+}]_i$ measurements (**Fig. 2d**). Thus, NO and reactive disulfides share a covalent modification site in TRPC5-channel protein complexes.

Free cysteine sulfhydryls are nitrosylated by NO (refs. 11,33) and are modified by reactive disulfides via disulfide exchange reactions in

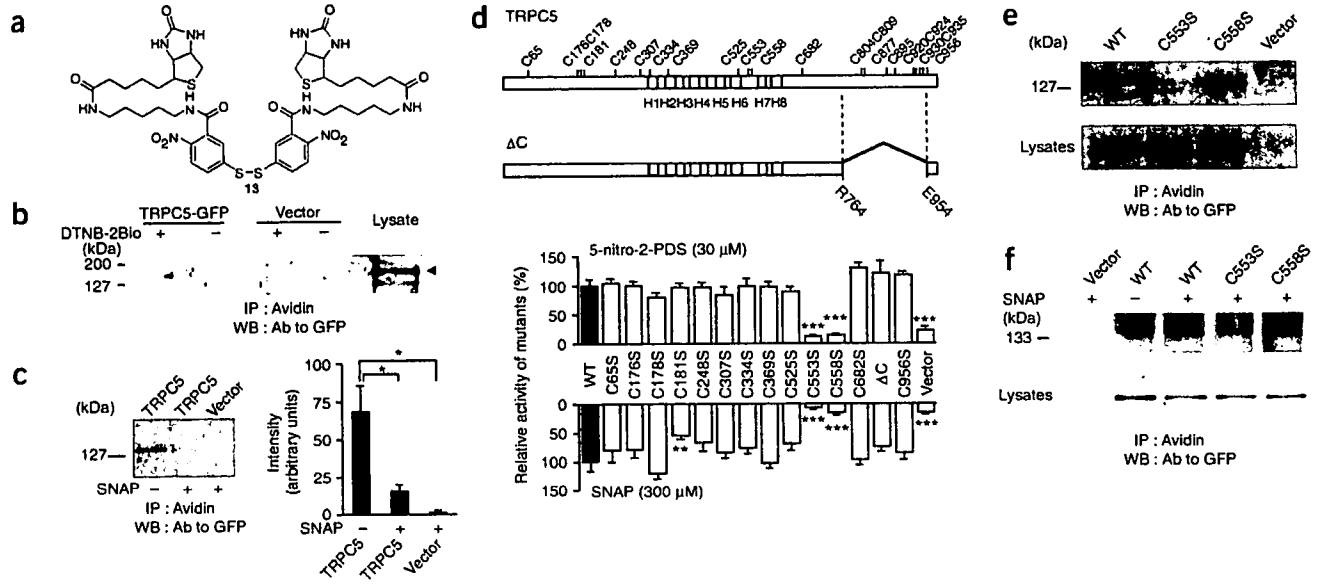

Figure 5 S-nitrosylation in TRPC5 channel protein complexes. (**a–c**) NO and reactive disulfides share incorporation site. (a) Chemical structure of DTNB-2Bio. (b) Detection of TRPC5-GFP among proteins incorporating DTNB-2Bio (100 μM) by western blot analysis (WB) using antibody to GFP. (c) Suppression of DTNB-2Bio incorporation by 5 mM SNAP (left); the total band intensity (right). Data points are mean ± s.e.m. $^*P < 0.05$. (d) Cysteine residues mapped on TRPC5 (top); cysteines were replaced with serine, or deleted in the ΔC mutant (in which Arg764 through Glu954 is deleted). Relative responses to 5-nitro-2-PDS ($n = 15–48$) and to SNAP ($n = 14–31$) of TRPC5 mutants in HEK cells (bottom). $^{**}P < 0.01$, $^{***}P < 0.001$, compared to WT. (e) Effects of mutations C553S and C558S on DTNB-2Bio incorporation. WB of total cell lysates indicates comparable TRPC5 expression (lysates). (f) Cysteine S-nitrosylation of WT TRPC5-GFP and mutants C553S and C558S with and without SNAP treatment. IP, immunoprecipitation.

proteins[12]. Therefore, cysteine residues are the most likely modification-site candidate. We subjected every cysteine residue in TRPC5 to replacement with serine or to deletion, and then we tested the mutants for their responses to 5-nitro-2-PDS and NO (**Fig. 5d**). Mutations C553S and C558S abrogated TRPC5 responses to NO (5%, 16% and 16% of wild-type (WT) response for C553S, C558S and vector, respectively) and TRPC5 responses to 5-nitro-2-PDS (13%, 15% and 24% of WT for C553S, C558S and vector, respectively). The resistance of the mutants is not attributable to localization defects, as the mutants showed intact plasma-membrane expression (like the WT protein) in assays using the biotinylation labeling method and in observations using an evanescent wave microscope that illuminates only the subcellular area from the surface to a depth of less than 100 nm by total internal reflection (**Supplementary Fig. 4** online). TRPC5 responses to receptor stimulations were only partially suppressed by C553S and C558S mutants (**Supplementary Fig. 4**), in contrast to TRPC5 responses to NO. The DTNB-2Bio incorporation was also abolished by C553S, whereas it was unaffected by C558S (**Fig. 5e**). Cysteine S-nitrosylation detected after selective conversion into biotinylated cysteines[10] was substantially enhanced by SNAP in WT proteins (184% ± 45% of basal level). TRPC5 nitrosylation was significantly suppressed by C553S (38% ± 21% of WT with SNAP) but was suppressed less extensively by C558S (75% ± 9.7% of WT with SNAP) (**Fig. 5f**). These results indicate that Cys553 is a main nitrosylation site and a predominant modification site for reactive disulfides.

TRP channels with conserved cysteines are responsive to NO

We tested NO-sensitive channel activation for generality in the TRP superfamily (**Fig. 6**). Notably, the alignment of amino acid sequences surrounding Cys553 and Cys558 of TRPC5 with counterpart sequences shows that TRPC5's closest relatives, TRPC1 and TRPC4, as well as thermosensor channels TRPV1, TRPV3 and TRPV4, have cysteines conserved on the N-terminal side of the putative pore-forming region H7 in the linker region located between the fifth and sixth transmembrane domains S5 and S6 (the S5-S6 linker) (**Fig. 6a**)[30,34]. TRPC1, TRPC4 and TRPV1 contain two cysteines separated by four residues (like TRPC5), whereas TRPV3 and TRPV4 have two and four cysteines, respectively, in sequences distantly related to TRPC5. These cysteines predict the NO responsiveness of these TRPC and TRPV channels to cysteine modifications.

We tested the recombinants of the above TRP protein homologs for susceptibility to SNAP, 5-nitro-2-PDS and H_2O_2 in HEK cells (**Fig. 6c–h**). As shown in **Figure 1**, the differences in maximal $[Ca^{2+}]_i$ rises (ΔF340/F380) statistically tested between control cells and the total populations of cells expressing TRPC1 or TRPC4β (a splice isoform of TRPC4) alone were not significant. However, in response to SNAP (300 μM) and 5-nitro-2-PDS (30 μM), a larger fraction (7%–9%) of expressing cells showed ΔF340/F380 > 0.5 relative to control cells (2%–5%). Cells co-expressing TRPC4β and TRPC5 showed SNAP and 5-nitro-2-PDS responses comparable to those in cells expressing TRPC5 alone (**Fig. 6c,d**), whereas cells co-expressing TRPC1 and TRPC5 showed slightly suppressed (yet robust) responses (**Fig. 6f,g**). In cells co-expressing TRPC5 and TRPC4β (**Fig. 6e**) or TRPC1 (**Fig. 6h**), H_2O_2 (1 mM) evoked significantly (TRPC1, $P = 0.003$; TRPC4, $P = 0.001$) impaired responses. We immunoprecipitated TRPC5 with co-expressed TRPC1 or TRPC4β (**Fig. 6b**) and the results suggest that heteromultimeric TRPC5/TRPC1 and TRPC5/TRPC4β channels have intact NO sensitivity and H_2O_2 resistance, whereas homomultimetric TRPC5 is sensitive to both NO and H_2O_2.

We also observed activation by NO for thermosensor channels TRPV1, TRPV3 and TRPV4, as predicted (**Fig. 7**). The augmentation of $[Ca^{2+}]_i$ rises by extracellular Ca^{2+} revealed NO- and 5-nitro-2-PDS–activated Ca^{2+} entry via TRPV1, TRPV3 and TRPV4

(Fig. 7a,b,d,e). TRPV1 and TRPV4 were responsive to H_2O_2, but TRPV3 was relatively resistant, much like the heteromultimeric TRPC channels (Fig. 6e,h and Fig. 7c,f). The TRPV1 mutant having substitutions at Cys616 and Cys621 (V1 mut) showed significantly (P = 0.005–0.031) suppressed responses to NO and other agents (Fig. 7d–f), and to nitrosylation (Fig. 7g). Notably, the H^+ sensitivity and heat sensitivity of TRPV1 was enhanced by NO (Fig. 7h,i). This enhancement was abolished by the mutation, whereas H^+ and heat responses without SNAP application (Fig. 7h,i) and surface expression (Supplementary Fig. 4) of the mutant were intact. Thus, channel activation regulated by nitrosylation is conserved among several TRP proteins.

Native TRP channels are activated by NO in endothelial cells

We characterized native Ca^{2+} influx triggered in response to NO in vascular endothelial cells (Figs. 8 and 9). As reported[20,35], cultured bovine aortic endothelial cells (BAEC) showed substantial enhancements of TRPC5 protein expression (Fig. 8a) and Ca^{2+} responses after 3 d of culture (Supplementary Fig. 5 online). To resolve involvements of TRPC5 in native Ca^{2+} influx, we measured $[Ca^{2+}]_i$ rises upon readdition of extracellular Ca^{2+} under agent stimulation after introducing TRPC5-selective small interference RNA (siTRPC5) and the dominant negative construct of TRPC5 (TRPC5-DN)[36] in BAEC. Ca^{2+} influx evoked by NO and 5-nitro-2-PDS was significantly suppressed by siTRPC5 and TRPC5-DN in BAEC (Fig. 9a,b). In contrast, H_2O_2 induced only marginal Ca^{2+} influx that was insensitive to siTRPC5 and TRPC5-DN (Fig. 9c). This activator sensitivity is similar to that observed in recombinant TRPC5/TRPC1 and TRPC5/TRPC4β heteromultimers in HEK cells (Fig. 6c–h) and is consistent with confocal immunoimages showing superimposable distribution of TRPC5 with TRPC1 and TRPC4 at the plasma membrane area

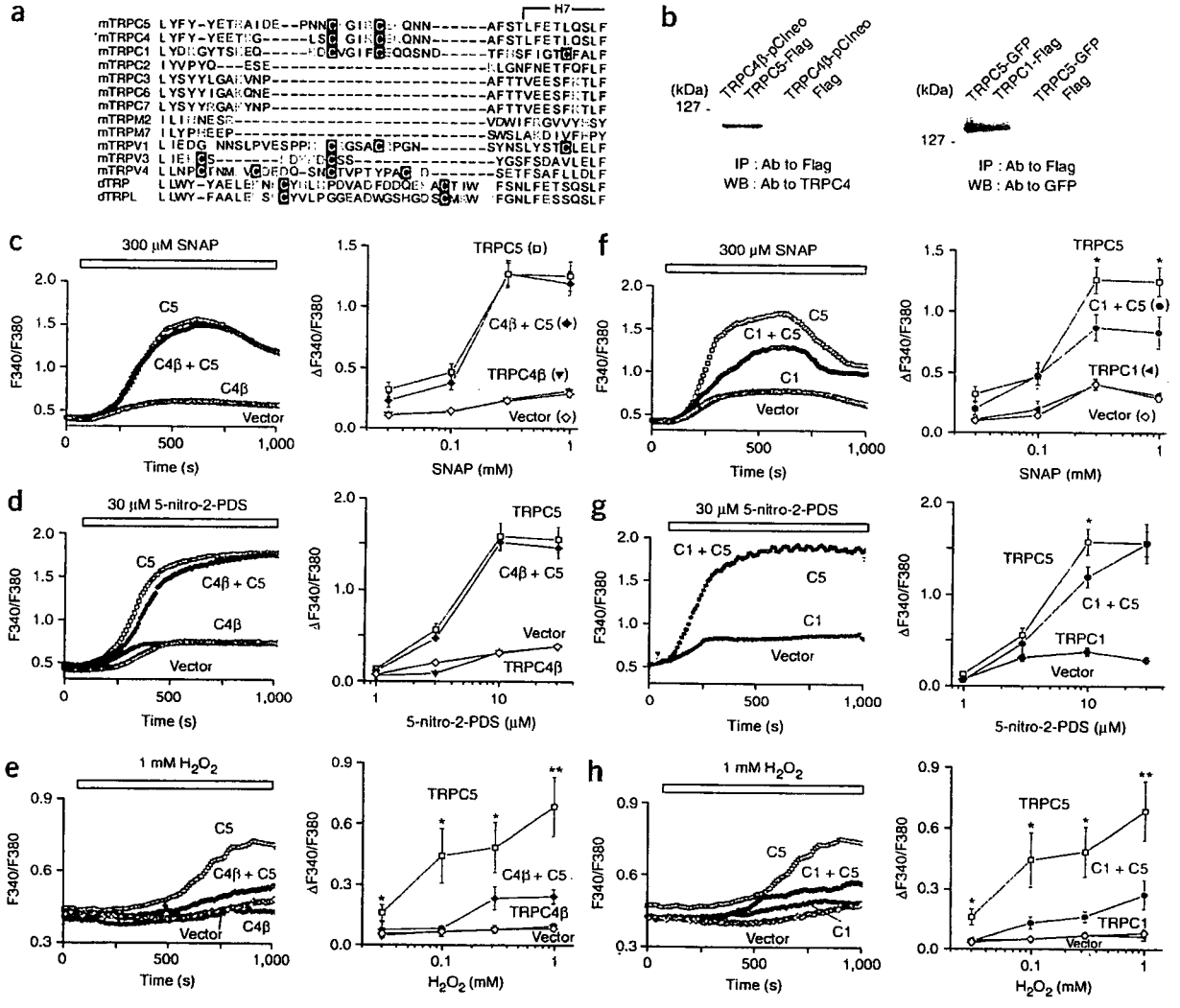

Figure 6 Molecular conservation of NO-induced activation in TRP channels. (a) Conserved cysteine residues on the N-terminal side of putative pore-forming regions in mouse TRPC1, TRPC2, TRPC3, TRPC4, TRPC5, TRPC6, TRPC7, TRPM2, TRPM7, TRPV1, TRPV3 and TRPV4 and *D. melanogaster* TRP and TRPL. (b) Co-immunoprecipitation of TRPC5 with TRPC4β (top) and TRPC1 (bottom). Immunoprecipitates (IP) with antibody to Flag from HEK cells expressing TRPC4β/TRPC5-Flag or TRPC1-Flag/TRPC5-GFP were subjected to WB with antibody to TRPC4 or GFP, respectively. pCIneo is the mammalian expression plasmid. (c–h) Ca^{2+} responses mediated by TRPC4β/TRPC5 (c–e) and TRPC1/TRPC5 heteromultimers (f–h) in HEK cells: average time courses of responses to SNAP (c,f), 5-nitro-2-PDS (d,g) and H_2O_2 (e,h) (left) and dose-response relationships (n = 21–49) (right). Data points are mean ± s.e.m. $^*P < 0.05$ and $^{**}P < 0.01$ for TRPC5, compared to TRPC5/TRPC4 or TRPC5/TRPC1.

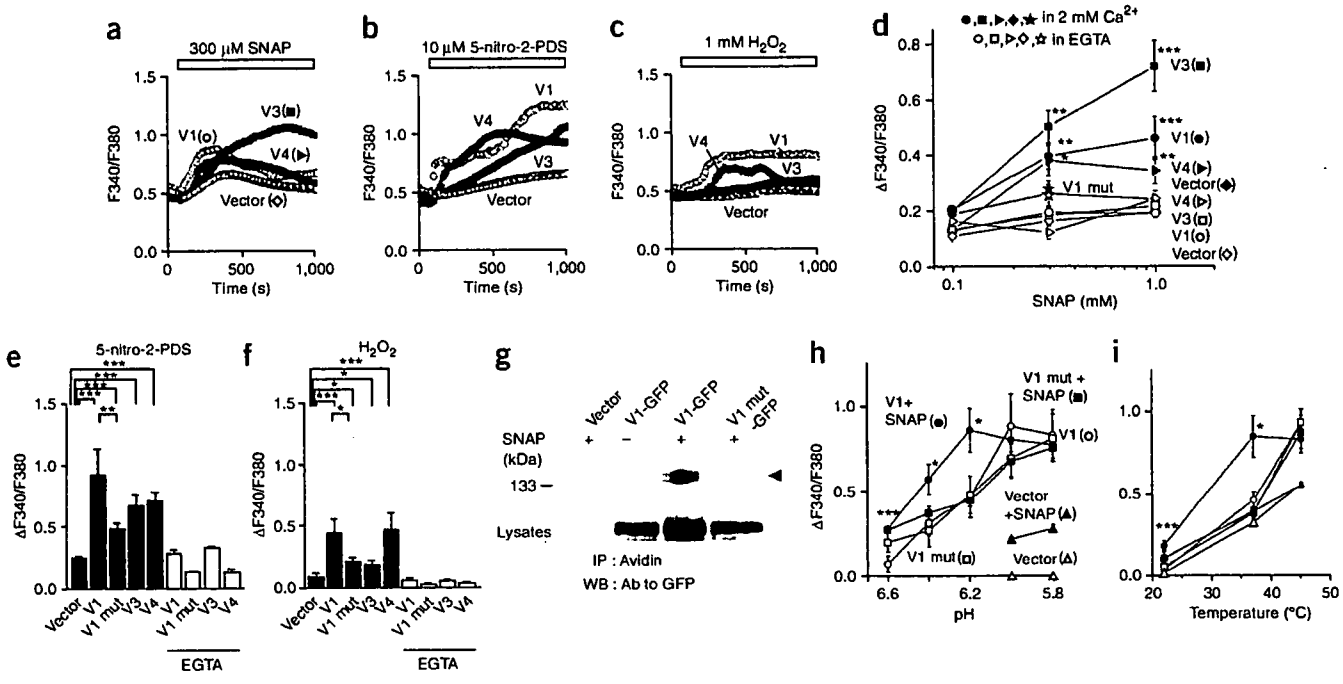

Figure 7 Regulation of TRPV channel activation by nitrosylation. (a–f) Ca^{2+} responses to SNAP (a), 5-nitro-2PDS (b) and H_2O_2 (c) mediated by rat TRPV1 and its cysteine substitution C616W C621S mutant (V1 mut), and human TRPV3 and TRPV4: average time courses (a–c), SNAP dose-response relationships (d), and maximal $[Ca^{2+}]_i$ rises by 5-nitro-2-PDS (e) and H_2O_2 (f) in the presence and absence (EGTA) of 2 mM external Ca^{2+} (n = 12–122). Data points are mean ± s.e.m. $^*P < 0.05$, $^{**}P < 0.01$ and $^{***}P < 0.001$ compared to control (vector). (g) S-nitrosylation of TRPV1-GFP and the mutant. (h,i) NO enhances H^+ and temperature sensitivity of TRPV1: effects of SNAP (300 μM) on pH (h) and temperature dependence (i) of responses mediated by TRPV1 and the mutant are shown (n = 7–50). $^*P < 0.05$ and $^{***}P < 0.001$, compared to TRPV1 in the absence of SNAP.

(Fig. 8b,c). Thus, heteromultimeric TRPC5/TRPC1 and TRPC5/TRPC4 channels are likely to conduct native NO-activated Ca^{2+} influx in endothelial cells.

ATP is a vasodilator that activates G protein–coupled receptors, which results in endothelial NO production via eNOS (ref. 16). We tested whether the NO produced by this physiological stimulation activates Ca^{2+} influx in BAEC. ATP induced $[Ca^{2+}]_i$ rises due to Ca^{2+} release in the absence of extracellular Ca^{2+} and those due to Ca^{2+} influx after the readmission of external Ca^{2+} (Fig. 9d). The NOS inhibitor N^{ω}-nitro-L-arginine methylester (L-NAME, 14) failed to affect Ca^{2+} release but significantly ($P < 0.001$) suppressed the Ca^{2+} influx (Fig. 9d) and NO production (Supplementary Fig. 5).

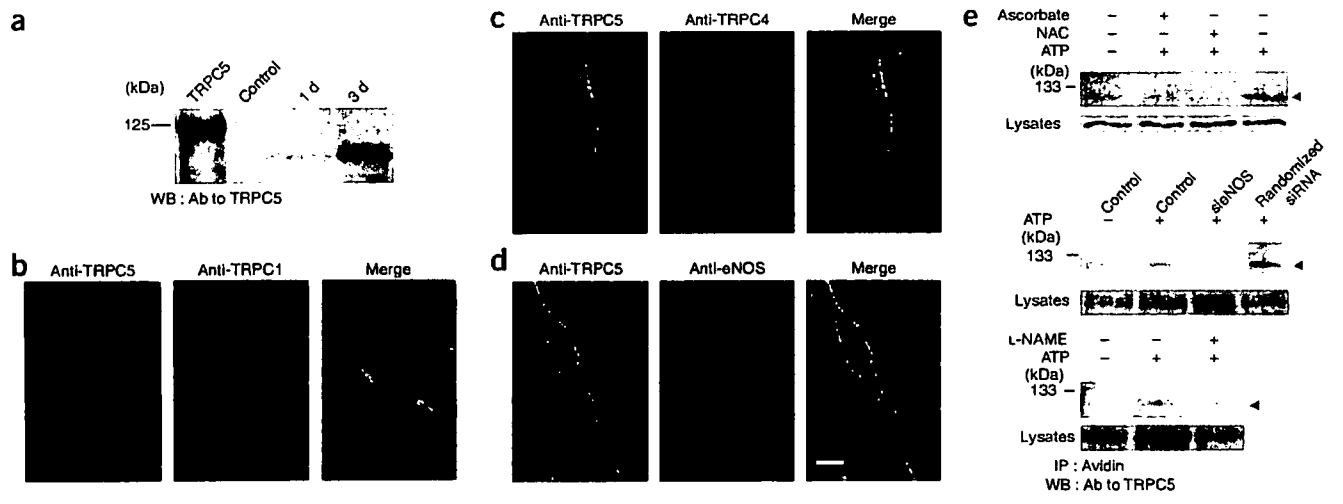

Figure 8 Physiological S-nitrosylation of native TRPC5 proteins in cultured endothelial cells. (a) WB reveals that TRPC5 protein expression is enhanced after a 3-d culture in BAEC. (b–d) Confocal fluorescence immunoimages of TRPC5 (green), TRPC1 (b), TRPC4 (c) and eNOS (d) (all red), and overlay of images (yellow) in BAECs. The bar indicates 10 μm. (e) S-nitrosylation of native TRPC5 by ATP receptor stimulation, and its inhibition by NAC and ascorbate (top), sieNOS (middle) and L-NAME (bottom) in BAECs.

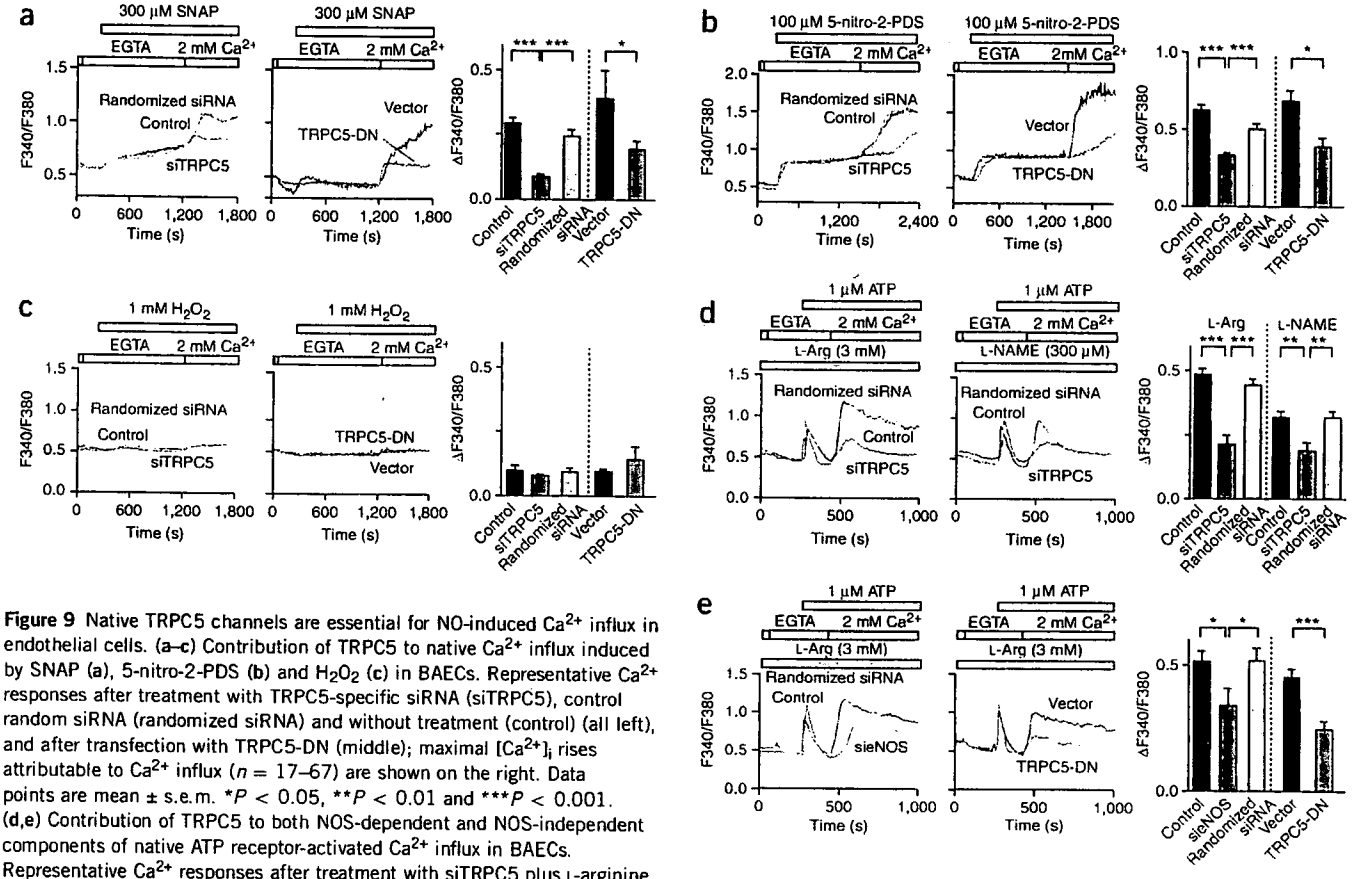

Figure 9 Native TRPC5 channels are essential for NO-induced Ca^{2+} influx in endothelial cells. (**a–c**) Contribution of TRPC5 to native Ca^{2+} influx induced by SNAP (**a**), 5-nitro-2-PDS (**b**) and H_2O_2 (**c**) in BAECs. Representative Ca^{2+} responses after treatment with TRPC5-specific siRNA (siTRPC5), control random siRNA (randomized siRNA) and without treatment (control) (all left), and after transfection with TRPC5-DN (middle); maximal $[Ca^{2+}]_i$ rises attributable to Ca^{2+} influx (n = 17–67) are shown on the right. Data points are mean ± s.e.m. $^*P < 0.05$, $^{**}P < 0.01$ and $^{***}P < 0.001$. (**d,e**) Contribution of TRPC5 to both NOS-dependent and NOS-independent components of native ATP receptor-activated Ca^{2+} influx in BAECs. Representative Ca^{2+} responses after treatment with siTRPC5 plus L-arginine (left) and L-NAME (middle) (**d**), and after suppression by sieNOS (left) and TRPC5-DN (middle) (**e**); maximal Ca^{2+} rises attributable to Ca^{2+} influx (**d**, n = 50–94; **e**, n = 21–38) are shown on the right. $^*P < 0.05$, $^{**}P < 0.01$ and $^{***}P < 0.001$.

This result, together with similar effects elicited by eNOS-targeted siRNA (sieNOS) (**Fig. 9e** and **Supplementary Fig. 5**) and by NO quencher *N*-acetyl-L-cysteine (NAC, **15**) and *S*-nitrosocysteine-selective reducing agent ascorbate (**Supplementary Fig. 5**), indicates a critical role for endogenous eNOS in inducing ATP receptor–activated Ca^{2+} influx. siTRPC5 more extensively diminished the Ca^{2+} influx and abolished the L-NAME sensitivity (**Fig. 9d**), which suggests that TRPC5 is essential for Ca^{2+} influx activated by NO via eNOS upon receptor stimulation. TRPC5-DN, which can also exert a suppressive effect on Ca^{2+} influx via nitrosylated TRPC5 (**Supplementary Fig. 1**), similarly suppressed the Ca^{2+} influx (**Fig. 9e**). In BAEC, siTRPC5 by contrast revealed lack of involvement of TRPC5 in SOC (**Supplementary Fig. 5**). Native TRPC5 proteins were susceptible to the suppression of ATP receptor–induced nitrosylation by ascorbate, L-NAME, NAC and sieNOS (**Fig. 8e** and **Supplementary Fig. 5**). Furthermore, confocal immunoimages indicate localization of TRPC5 with eNOS (**Fig. 8d**). These results provide evidence for activation of native TRPC5 channels by nitrosylation via eNOS upon ATP receptor stimulation in endothelial cells.

DISCUSSION

The present study describes a previously unknown activation mechanism of TRP channels via cysteine S-nitrosylation, as well as a structural motif essential for the activation gating. Among TRPCs coupled to PLC-linked receptors, TRPC5 showed prominent sensitivity to NO, and nitrosylated Cys553 and Cys558 mediated the responsiveness in TRPC5. A critical contribution of native nitrosylated TRPC5 to Ca^{2+} entry was revealed by siRNA and dominant negative suppression in endothelial cells. Notably, TRPC1 and TRPC4β associated with TRPC5, and thermosensors TRPV1, TRPV3 and TRPV4, which have cysteines nearby the same putative pore-forming region, responded well to NO. These TRPC and TRPV channels may comprise a new TRP protein category whose members serve as ubiquitous cell-surface NO sensors that are essential for integrating NO and Ca^{2+} signals.

The data (**Fig. 4**) suggest that NO and reactive disulfides exert their actions independently of receptor-induced cascades or Ca^{2+} store depletion in activating TRPC5. In fact, SNAP (at low concentrations) and reactive disulfides failed to activate TRPC2, TRPC3, TRPC6 and TRPC7, which are all activated by receptor stimulation[2–7]. SNAP also failed to significantly affect endogenous SOCs in HEK cells (**Supplementary Fig. 1**). The abolishment of DTNB-2Bio incorporation by SNAP co-application and by the C553S TRPC5 mutation, and the suppression of nitrosylation by the C553S mutation (**Fig. 5**), further indicate that both NO and reactive disulfides directly modify Cys553 in the TRPC5 protein. Compared to C553S, C558S weakly reduced nitrosothiol concentrations. This, together with the partial resistance of NO-induced TRPC5 response to ascorbate (**Fig. 3a**) may suggest that the free sulfhydryl group of Cys558 nucleophilically attacks nitrosylated Cys553 to form a disulfide bond that stabilizes the open state. S-nitrosylation activates the ryanodine receptor channel[37] and cyclic nucleotide-gated cation channels[38], and it modulates NMDA receptors[33]. Ryanodine receptors are also activated by reactive

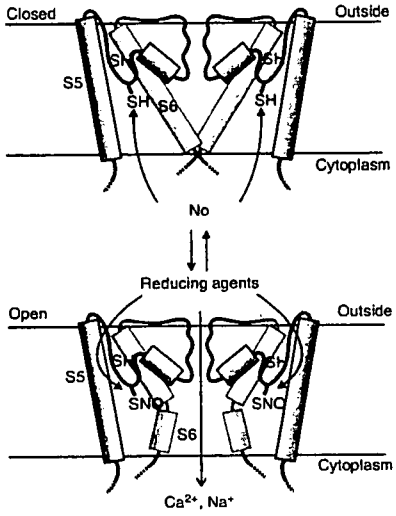

Figure 10 Model for TRP channel activation by NO and reactive disulfides. Possible protein conformation change during activation of TRPC5 channels by NO is shown. The activation trigger NO modifies the free sulfhydryl group of Cys553 that is accessible from the cytoplasmic side. This direct thiol S-nitrosylation induces a bend of S6 that opens the intracellular activation gate. The cysteine modification is reversed by the hydrophilic reducing agents DTT and ascorbate applied externally. SNO, *S*-nitrosothiol.

disulfides[12]. In proteins with high NO sensitivity, basic and acidic amino acids surrounding S-nitrosylated cysteines[11] have been proposed to enhance the nucleophilicity of sulfhydryl and its S-nitrosylation, as reported in acid-base catalysis of hemoglobin nitrosylation. In this context, charged residues flanking Cys553 and Cys558 (**Fig. 6a**) may confer modification susceptibility to their free sulfhydryls and to the free sulfhydryls of their counterpart cysteines in TRPC and TRPV channels, which are commonly distinguished on the basis of their characteristic activation triggers: receptor activation and heat, respectively. Notably, so-called thermoTRPs are comprised of members of several TRP protein families (TRPV, TRPM and TRPA)[3–5]. Therefore, together with NO-activated TRP proteins, thermoTRPs[3–5] can be considered as one of the few functional categories that extends over several TRP protein families. Our findings may provide the first clear chemical biological basis for TRP categorization of this hierarchy.

Our results suggest that NO and reactive disulfides selectively modify Cys553 and Cys558 residues that are coupled to the gating apparatus in functionally critical domains of the TRPC5 protein. Because C553S and C558S mutations of TRPC5 only partially suppress receptor-induced TRPC5 responses (**Supplementary Fig. 4**), the cysteines are not absolute necessities but probably have an important regulatory role in TRPC5 activation. Intact receptor-induced responses after DTT treatment (unpublished data) further suggest that the oxidative cysteine modifications are not required for receptor stimulation to activate TRPC5. In TRPV1, the cysteine mutation that impaired NO sensitivity failed to affect H^+ and temperature sensitivities under the control condition in the absence of NO. Therefore, the role played by the nitrosylation-target cysteines in H^+- and heat-induced activation of TRPV1 may be qualitatively comparable to the regulatory role played by the counterpart cysteines in receptor-induced activation of TRPC5, assuming quantitative differences between the mutations in severity of functional impairments attributable to structural changes.

Surprisingly, despite the location of Cys553 and Cys558 in the extracellularly disposed S5-S6 linker (according to previous studies[34]), the modifications are unlikely to affect the structure of the ion-conducting pore, as similar single-channel conductances are observed for the spontaneously activated TRPC5 channel (47.6 pS)[39] and the 5-nitro-2-PDS–activated TRPC5 channel (44.1 pS). Moreover, the sidedness of action of DTNB and the time lags preceding the responses after agent application support the hypothesis that modification agents access from the cytoplasmic side to open the intracellular activation gate of TRPC5 channels (**Fig. 10**). In *D. melanogaster* Shaker voltage-gated K^+ channels, the activation gate formed by S6 residues near the intracellular entrance of the pore cavity has been identified[31]. Considering the longer S5-S6 linkers of TRPC5, TRPC1 and TRPC4, which are comprised of approximately 60 residues (in comparison with 50 residues in TRPC2, TRPC3, TRPC6 and TRPC7 and 40 residues in the Shaker K^+ channel), the TRPC5 S5-S6 linker with modified Cys553 may be invaginated toward the cytoplasm to reach the S6 activation gate (**Fig. 10**). However, external DTT and ascorbate reversed the TRPC5 activation (**Fig. 3a,b** and **Supplementary Fig. 2**), and in TRPV1 the cysteine counterparts have been suggested as sites for blockade by externally applied oxidizing agents[40,41]; also, an antibody raised against a peptide containing Cys553 at the C terminus inhibits TRPC5 activity[42]. Therefore, Cys553 is very likely located at the interface between the inside and outside of the cell.

The plasma-membrane expression of TRPC5 unaffected by C553S, C558S or cellular stimulations except epidermal growth factor (**Supplementary Fig. 4**) may suggest minimal contribution of protein trafficking to NO-induced activation in HEK cells. However, involvements of protein recruitments through the fusion of vesicles with the plasma membrane and lateral movements within the plasma membrane cannot be excluded. Ca^{2+}-dependent BK-type K^+ channels are modulated by several mechanisms, such as redox-sensitive extracellular gates containing cysteine residues in the auxiliary β subunit[43] and heme bound to the pore-forming α subunit[44]. Therefore, conformational changes elicited by cysteine modification in an unidentified associated protein may be transmitted to TRPC5 via Cys553, if the protein association is maintained during the labeling assays. Thus, cysteine modifications may exert their action via multiple pathways on the pore-forming TRPC5 protein, which is consistent with the previously reported multiplicity of signals responsible for channel activation of TRPC5 (ref. 45).

Ca^{2+} influx via nitrosylated TRP channels may mediate the positive feedback regulation of Ca^{2+}-dependent NO production. In support of this view, native NO-activated Ca^{2+} channels have been reported in different systems including endothelial cells[24,25,46,47], in which cation currents are activated by glutathione disulfide[48]. However, suppressive effects of NO on Ca^{2+} entry have also been demonstrated in endothelial cells[26,27]. This discrepancy is at least in part attributable to diversity in NO susceptibility of ion channels and signaling pathways that regulate Ca^{2+} influx. In fact, Ca^{2+} entry via SOCs is potentiated indirectly by NO through the enhancement of Ca^{2+} release[23]. In endothelial cells in which cGMP mediates NO signals (for example, as observed in smooth muscle[26,27]), NO suppresses Ca^{2+} entry. Moreover, NO has been shown to inhibit NOS[11]. Thus, ensembles of multiple NO-regulated mechanisms may determine net Ca^{2+} entry. Notably, in the NMDA receptor Ca^{2+}-permeable channel NR1/NR2A, nNOS physically coupled to the NR1 subunit through the scaffolding protein PSD-95 nitrosylates the NR2A subunit to elicit feedback inhibition of channel activity[33]. To resolve the complexity in cross talk between NO and Ca^{2+} signals, precise identification of physiological protein interaction between nitrosylated TRP channels and NOSs is necessary.

Our immunolocalization studies have revealed that TRPC5 is distributed on both the apical and basal membranes in the endothelial cell layer of vascular tissue (unpublished data). Given that vasodilator receptors are distributed at the apical luminal surface of endothelial cell layers, NO that is initially produced there may diffuse across the cytoplasm and activate TRPC5 proteins located at the basolateral membrane. This may lead to an efficient propagation of Ca^{2+} signals vectorized toward the basal membrane. The feedback mechanism may further contribute to global $[Ca^{2+}]_i$ rises or oscillations and to full activation of eNOS at the Golgi in endothelial cells, thereby leading to synchronization of neighboring smooth muscle cells in vascular relaxation. Notably, TRPC5 is important in neurite extension[36]. Given that NO signals are reported to regulate neurite extension[49], the feedback mechanism may also be important in growth-cone morphology. In terms of TRPVs, our results may raise the possibility that nitrosylation-induced Ca^{2+} entry is involved in heat or pain sensation. Thus, the positive feedback regulation of Ca^{2+} signals by NO-activated TRP channels may be involved in diverse biological systems.

Impaired aortic vasorelaxation and reduced endothelial $[Ca^{2+}]_i$ increase upon agonist stimulation has been demonstrated in TRPC4-deficient mice[50]. These results are notable in the context of our study, considering that Cys553 and Cys558 counterparts are found in TRPC4. TRPC5/TRPC4β and TRPC5/TRPC1 channels had intact NO sensitivity and significant H_2O_2 resistance. These observations, together with our immunohistochemistry and co-immunoprecipitation experiments (**Figs. 6** and **8**), suggest that heteromultimerization with TRPC1 or TRPC4β may enable TRPC5 to maintain its NO-sensing function while acquiring resistance to the pathological action of reactive oxygen species[11,28] in endothelial cells. To understand the mechanism underlying this sensitivity, three-dimensional structural analysis and detailed studies of the binding pocket for the activation triggers using cysteine-modification agents of different sizes is critical.

METHODS

Cell culture and cDNA expression. The TRPC5 mutants were constructed using PCR techniques. TRPC1-Flag and TRPC5-Flag were first established in plasmid pCMV-Tag4 (Stratagene). The culture of HEK cells and chicken DT40 B lymphocytes, as well as cDNA expression, were performed as described previously[28,32]. BAECs were cultured in phenol red–free DMEM (Gibco) containing 10% FBS, 30 units ml^{-1} penicillin, 1 μM all-*trans*-retinoic acid and 30 μg ml^{-1} streptomycin at 37 °C under 5% CO_2. To remove retinoid hormones, FBS was incubated with 0.5% dextran-coated charcoal (Sigma) at 4 °C overnight. TRPC5-DN was transfected using Lipofectamine 2000 (Invitrogen). Cells were trypsinized and diluted by DMEM and plated onto glass coverslips 24 h after transfection. The cells were subjected to measurements 8–24 h after plating.

siRNA experiment. We used the sense siRNA sequences 5′-AATGCCTTCTCC ACGCTCTTT-3′ for bovine TRPC5 and 5′-AATATCCTGGAGGATGTGGCC-3′ for bovine eNOS. The randomized siRNA target sequences were 5′-AATCGC CTCTTACGCTCCTTT-3′ and 5′-AATGCGTGTTGCTAGACGCAG-3′, respectively. Computer analysis confirmed this sequence to be a specific target that does not have homology to other bovine genes. We used the Silencer siRNA Construction Kit (Ambion) to construct siRNA oligomers, and we transfected the siRNAs to cultured endothelial cells using Lipofectamine 2000.

Immunoprecipitation and western blot analysis. HEK cells ($\sim 3 \times 10^6$) transfected with TRPC4β with TRPC5-Flag, TRPC5-GFP with TRPC1-Flag, TRPC4β with pCMV-Tag4, and TRPC5-GFP with pCMV-Tag4 were lysed in 200 μl of RIPA buffer (pH 8.0) containing 150 mM NaCl, 1% Nonidet P-40, 0.5% sodium deoxycholate, 0.1% SDS, 50 mM Tris, 1 mM PMSF and 10 μg ml^{-1} leupeptin. TRPC5-Flag and TRPC1-Flag were immunoprecipitated with M2 monoclonal antibody to Flag (Sigma) in the presence of sepharose A-agarose beads (Amersham Pharmacia) rocked overnight at 4 °C. The immune complexes were washed eight times with RIPA buffer for 5 min at room temperature (22 ± 2 °C) and resuspended in SDS sample buffer. The protein samples were fractionated by 7.5% SDS-PAGE and electrotransferred onto a nitrocellulose membrane. The blots were incubated with an antibody to GFP (BD Biosciences) or an antibody to TRPC4 (Sigma) and stained using the enhanced chemiluminescence (ECL) system (Amersham Pharmacia). Cultured BAECs were subjected to western blot analysis using anti-mouse TRPC5 rabbit antiserum (H8C1) directed against the C terminus (682-CPKRDPDGRRRRHNLRS-698).

DTNB-2Bio labeling assay. DTNB-2Bio was synthesized by biotinylation of the two carboxyl groups of DTNB (Dojindo) using EZ-link 5-(Biotinamido) pentylamine (50 mg, Pierce) after converting DTNB to succinimidyl DTNB. HEK cells transfected with TRPC5-GFP or vector ($\sim 5 \times 10^6$) were washed by phosphate-buffered saline (PBS) three times. The surface membrane was permeabilized by exposure to HEPES-buffered saline (HBS) containing 0.01% digitonin for 5 min. The cells were collected and exposed to HBS containing 100 μM DTNB-2Bio for 20 min at room temperature. The cells were washed with PBS three times, harvested, and lysed in RIPA buffer. Cell lysates were incubated batch-wise with NeutrAvidin-Plus beads (Pierce) overnight at 4 °C with constant shaking. The beads were rinsed six times with RIPA buffer by centrifugation at 14,000 r.p.m. for 30 s. The proteins were eluted in sample buffer containing DTT (50 mM) at room temperature for 20 min and analyzed by 10% SDS-PAGE and western blot detection using an antibody to GFP.

S-nitrosylation assay. The S-nitrosylation assay (biotin switch assay) was performed as described previously[10] with a few modifications. HEK cells expressing TRPC5-GFP constructs were incubated with SNAP (5 mM) or with control DMSO in the dark at room temperature for 10 min, and BAECs were pretreated with ascorbate (10 mM), NAC (1 mM) for 15 min, or L-NAME (10 mM) for 32 h, and then exposed to ATP (1 μM) in the dark at room temperature for 5 min. The cells were washed with PBS two times, harvested, and lysed in RIPA buffer. The extracts were incubated with 100 mM methylmethanethiosulfonate (MMTS) and 2.5% SDS at 50 °C for 30 min, and MMTS was removed by precipitation with an equal volume of –30 °C acetone. After resuspending the proteins in HEN buffer (250 mM HEPES pH 7.7, 1 mM EDTA and 0.1 mM neocuproine) containing 1% SDS, we added sodium ascorbate (1 mM final concentration) and biotin-HPDP (1 mM final concentration, Pierce). The mixtures were incubated for 1 h at 25 °C in the dark with intermittent vortexing. Biotinylated nitrosothiols were then acetone-precipitated with 2 volumes of –30 °C acetone to remove residual biotin-HPDP. After centrifugation, the pellet was resuspended in 0.1 ml HEN buffer containing 1% SDS. Two volumes of neutralization buffer (20 mM HEPES, pH 7.7, 100 mM NaCl, 1 mM EDTA, 0.5% Triton X-100) were added, and biotinylated proteins were incubated with 20 μl of NeutrAvidin-Plus beads for 1 h at room temperature. The resin was extensively washed in 10 volumes of neutralization buffer containing 600 mM NaCl. The proteins were eluted in sample buffer containing DTT (50 mM) at room temperature for 30 min and analyzed by 7.5% SDS-PAGE and western blotting with an antibody to GFP to detect TRPC5-GFP or an antibody to TRPC5 (Alomone) to detect native bovine TRPC5.

Confocal immunovisualization in BAECs. Cultured BAECs were incubated for 1 h at room temperature with goat polyclonal antibody to TRPC5 (1:100) (Santa Cruz Biotech) plus each one of rabbit polyclonal antibodies to TRPC1 (1:100) (Sigma) and to TRPC4 (1:100) (Alomone), or plus mouse monoclonal antibody to eNOS (1:500) (Calbiochem) in PBS containing 5% BSA, and for 1 h with the fluorescein isothiocyanate (FITC)-conjugated anti-goat IgG to detect TRPC5, Cy3-conjugated anti-mouse IgG to detect eNOS and Cy3-conjugated anti-rabbit IgG to detect TRPC1 or TRPC4. The fluorescence images were acquired with a confocal laser-scanning microscope using the 488-nm line of an argon laser for excitation and a 505-nm to 525-nm band-pass filter for emission, or the 543-nm line of a HeNe laser for excitation and a 560-nm long-pass filter for emission. The specimens were viewed at high magnification using plan oil objectives (×60, 1.40 numerical aperture (NA), Olympus).

Fluorescent $[Ca^{2+}]_i$ measurements and electrophysiology. The fura-2 fluorescence was measured in HBS containing the following: NaCl, 107 mM; KCl,

6 mM; $MgSO_4$, 1.2 mM; $CaCl_2$, 2 mM; glucose, 11.5 mM; HEPES, 20 mM; adjusted to pH 7.4 with NaOH. The 340:380-nm ratio images were obtained on a pixel-by-pixel basis. Fura-2 measurements were carried out at 22 ± 1 °C using HBS adjusted to pH 7.4, or as otherwise stated. Whole-cell currents were recorded at room temperature using the conventional whole-cell mode of the patch clamp technique with EPC9 amplifier (Heka) as described previously[28]. The standard pipette-filling solution contained the following: CsOH, 105 mM; L-aspartate, 105 mM; CsCl, 40 mM; $CaCl_2$, 1.33 mM; $MgCl_2$, 2 mM; ethyleneglycol-bis(β-aminoethyl)-*N*,*N*,*N*′,*N*′-tetraacetic acid (EGTA, **16**), 5 mM; HEPES, 5 mM; Na_2ATP, 2 mM; adjusted to pH 7.25 with CsOH (50 nM calculated free Ca^{2+}). The 2-mM Ca^{2+}-NaCl solution contained: NaCl, 125 mM; $MgCl_2$, 1.2 mM; $CaCl_2$, 2 mM; glucose, 10 mM; HEPES, 11.5 mM; mannitol, 49 mM; adjusted to pH 7.4 with NaOH. The osmolarity of external solutions was adjusted to about 325 mosM. For the inside-out patch recording, the recording pipette contained the 2-mM Ca^{2+}-NaCl solution, and the bathing solution had the same composition as standard pipette-filling solution. Recordings were filtered at 1 kHz. Linear regression was used to yield a single-channel conductance from *I–V* relationship.

Statistical analysis. All data are expressed as means ± s.e.m. The data were accumulated under each condition from at least three independent experiments. The statistical analyses were performed using the Student's *t*-test.

Additional methods. Further details of cell culture, complementary DNA expression, synthesis of DTNB-2Bio, confocal immunovisualization of proteins, and fluorescence and electrophysiological measurements are in **Supplementary Methods** online.

Accession codes. GenBank: bovine TRPC5, XM_617015; bovine eNOS, NM_181037.

Note: Supplementary information is available on the Nature Chemical Biology website.

ACKNOWLEDGMENTS

We thank D.E. Clapham and C. Strubing for TRPC5-DN, T. Furukawa and M. Nishida for helpful discussions, E. Mori and M. Sasaki for expert experiments and T. Kurosaki for IP_3 receptor–deficient DT40 cells. This study was supported by research grants from the Ministry of Education, Culture, Sports, Science and Technology of Japan, the Japan Society for the Promotion of Science, and from the Mitsubishi Foundation.

AUTHOR CONTRIBUTIONS

T.Y., acquisition, analysis and interpretation of data, and drafting and revision of the manuscript; N.T., S.Y., Y.H., R.I., T.M., M.T., S.S. and Y.S., acquisition, analysis and interpretation of data; Y.M., analysis and interpretation of data, and drafting and critical review of the manuscript.

COMPETING INTERESTS STATEMENT

The authors declare that they have no competing financial interests.

Published online at http://www.nature.com/naturechemicalbiology
Reprints and permissions information is available online at http://npg.nature.com/reprintsandpermissions/

1. Berridge, M.J., Bootman, M.D. & Lipp, P. Calcium—a life and death signal. *Nature* **395**, 645–648 (1998).
2. Montell, C., Birnbaumer, L. & Flockerzi, V. The TRP channels, a remarkably functional family. *Cell* **108**, 595–598 (2002).
3. Clapham, D.E. TRP channels as cellular sensors. *Nature* **426**, 517–524 (2003).
4. Voets, T., Talavera, K., Owsianik, G. & Nilius, B. Sensing with TRP channels. *Nat. Chem. Biol.* **1**, 85–92 (2005).
5. Clapham, D.E., Julius, D., Montell, C. & Schultz, G. International Union of Pharmacology. XLIX. Nomenclature and structure-function relationships of transient receptor potential channels. *Pharmacol. Rev.* **57**, 427–450 (2005).
6. Zhu, X. *et al. trp*, a novel mammalian gene family essential for agonist-activated capacitative Ca^{2+} entry. *Cell* **85**, 661–671 (1996).
7. Vazquez, G., Wedel, B.J., Aziz, O., Trebak, M. & Putney, J.W., Jr. The mammalian TRPC cation channels. *Biochim. Biophys. Acta* **1742**, 21–36 (2004).
8. Caterina, M.J. *et al.* The capsaicin receptor: a heat-activated ion channel in the pain pathway. *Nature* **389**, 816–824 (1997).
9. Patapoutian, A., Peier, A.M., Story, G.M. & Viswanath, V. Thermo TRP channels and beyond: mechanisms of temperature sensation. *Nat. Rev. Neurosci.* **4**, 529–539 (2003).
10. Jaffrey, S.R., Erdjument-Bromage, H., Ferris, C.D., Tempst, P. & Snyder, S.H. Protein S-nitrosylation: a physiological signal for neuronal nitric oxide. *Nat. Cell Biol.* **3**, 193–197 (2001).
11. Hess, D.T., Matsumoto, A., Kim, S.O., Marshall, H.E. & Stamler, J.S. Protein S-nitrosylation: purview and parameters. *Nat. Rev. Mol. Cell Biol.* **6**, 150–166 (2005).
12. Zaidi, N.F., Lagenaur, C.F., Abramson, J.J., Pessah, I. & Salama, G. Reactive disulfides trigger Ca^{2+} release from sarcoplasmic reticulum via an oxidation reaction. *J. Biol. Chem.* **264**, 21725–21736 (1989).
13. Moncada, S., Higgs, A. & Furchgott, R. International Union of Pharmacology nomenclature in nitric oxide research. *Pharmacol. Rev.* **49**, 137–142 (1997).
14. Venema, V.J. *et al.* Bradykinin stimulates the tyrosine phosphorylation and bradykinin B2 receptor association of phospholipase Cγ1 in vascular endothelial cells. *Biochem. Biophys. Res. Commun.* **246**, 70–75 (1998).
15. Zachary, I. & Gliki, G. Signaling transduction mechanisms mediating biological actions of the vascular endothelial growth factor family. *Cardiovasc. Res.* **49**, 568–581 (2001).
16. Koyama, T., Kimura, C., Park, S.J., Oike, M. & Ito, Y. Functional implications of Ca^{2+} mobilizing properties for nitric oxide production in aortic endothelium. *Life Sci.* **72**, 511–520 (2002).
17. Hutcheson, I.R. & Griffith, T.M. Central role of intracellular calcium stores in acute flow- and agonist-evoked endothelial nitric oxide release. *Br. J. Pharmacol.* **122**, 117–125 (1997).
18. Lantoine, F., Iouzalen, L., Devynck, M.A., Millanvoye-Van Brussel, E. & David-Dufilho, M. Nitric oxide production in human endothelial cells stimulated by histamine requires Ca^{2+} influx. *Biochem. J.* **330**, 695–699 (1998).
19. Lin, S. *et al.* Sustained endothelial nitric-oxide synthase activation requires capacitative Ca^{2+} entry. *J. Biol. Chem.* **275**, 17979–17985 (2000).
20. Yao, X. & Garland, C.J. Recent developments in vascular endothelial cell transient receptor potential channels. *Circ. Res.* **97**, 853–863 (2005).
21. Mungrue, I.N. & Bredt, D.S. nNOS at a glance: implications for brain and brawn. *J. Cell Sci.* **117**, 2627–2629 (2004).
22. Khan, S.A. & Hare, J.M. The role of nitric oxide in the physiological regulation of Ca^{2+} cycling. *Curr. Opin. Drug Discov. Devel.* **6**, 658–666 (2003).
23. Volk, T., Mäding, K., Hensel, M. & Kox, W.J. Nitric oxide induces transient Ca^{2+} changes in endothelial cells independent of cGMP. *J. Cell. Physiol.* **172**, 296–305 (1997).
24. Chen, J. *et al.* Autocrine action and its underlying mechanism of nitric oxide on intracellular Ca^{2+} homeostasis in vascular endothelial cells. *J. Biol. Chem.* **275**, 28739–28749 (2000).
25. Li, N., Sul, J.Y. & Haydon, P.G. A calcium-induced calcium influx factor, nitric oxide, modulates the refilling of calcium stores in astrocytes. *J. Neurosci.* **23**, 10302–10310 (2003).
26. Kwan, H.Y., Huang, Y. & Yao, X. Store-operated calcium entry in vascular endothelial cells is inhibited by cGMP via a protein kinase G-dependent mechanism. *J. Biol. Chem.* **275**, 6758–6763 (2000).
27. Dedkova, E.N. & Blatter, L.A. Nitric oxide inhibits capacitative Ca^{2+} entry and enhances endoplasmic reticulum Ca^{2+} uptake in bovine vascular endothelial cells. *J. Physiol. (Lond.)* **539**, 77–91 (2002).
28. Hara, Y. *et al.* LTRPC2 Ca^{2+}-permeable channel activated by changes in redox status confers susceptibility to cell death. *Mol. Cell* **9**, 163–173 (2002).
29. Aarts, M. *et al.* A key role for TRPM7 channels in anoxic neuronal death. *Cell* **115**, 863–877 (2003).
30. Okada, T. *et al.* Molecular cloning and functional characterization of a novel receptor-activated TRP Ca^{2+} channel from mouse brain. *J. Biol. Chem.* **273**, 10279–10287 (1998).
31. del Camino, D. & Yellen, G. Tight steric closure at the intracellular activation gate of a voltage-gated K^+ channel. *Neuron* **32**, 649–656 (2001).
32. Sugawara, H., Kurosaki, M., Takata, M. & Kurosaki, T. Genetic evidence for involvement of type 1, type 2 and type 3 inositol 1,4,5-trisphosphate receptors in signal transduction through the B-cell antigen receptor. *EMBO J.* **16**, 3078–3088 (1997).
33. Choi, Y.B. *et al.* Molecular basis of NMDA receptor-coupled ion channel modulation by S-nitrosylation. *Nat. Neurosci.* **3**, 15–21 (2000).
34. Vannier, B., Zhu, X., Brown, D. & Birnbaumer, L. The membrane topology of human transient receptor potential 3 as inferred from glycosylation-scanning mutagenesis and epitope immunocytochemistry. *J. Biol. Chem.* **273**, 8675–8679 (1998).
35. Chang, A.S., Chang, S.M., Garcia, R.L. & Schilling, W.P. Concomitant and hormonally regulated expression of *trp* genes in bovine aortic endothelial cells. *FEBS Lett.* **415**, 335–340 (1997).
36. Greka, A., Navarro, B., Oancea, E., Duggan, A. & Clapham, D.E. TRPC5 is a regulator of hippocampal neurite length and growth cone morphology. *Nat. Neurosci.* **6**, 837–845 (2003).
37. Xu, L., Eu, J.P., Meissner, G. & Stamler, J.S. Activation of the cardiac calcium release channel (ryanodine receptor) by poly-S-nitrosylation. *Science* **279**, 234–237 (1998).
38. Broillet, M.C. & Firestein, S. Direct activation of the olfactory cyclic nucleotide-gated channel through modification of sulfhydryl groups by NO compounds. *Neuron* **16**, 377–385 (1996).
39. Yamada, H. *et al.* Spontaneous single-channel activity of neuronal TRP5 channel recombinantly expressed in HEK293 cells. *Neurosci. Lett.* **285**, 111–114 (2000).
40. Jin, Y. *et al.* Thimerosal decreases TRPV1 activity by oxidation of extracellular sulfhydryl residues. *Neurosci. Lett.* **369**, 250–255 (2004).
41. Tousova, K., Susankova, K., Teisinger, J., Vyklicky, L. & Vlachova, V. Oxidizing reagent copper-*o*-phenanthroline is an open channel blocker of the vanilloid receptor TRPV1. *Neuropharmacology* **47**, 273–285 (2004).

42. Xu, S.Z. *et al.* Generation of functional ion-channel tools by E3 targeting. *Nat. Biotechnol.* **23**, 1289–1293 (2005).
43. Zeng, X.H., Xia, X.M. & Lingle, C.J. Redox-sensitive extracellular gates formed by auxiliary β subunits of calcium-activated potassium channels. *Nat. Struct. Biol.* **10**, 448–454 (2003).
44. Tang, X.D. *et al.* Haem can bind to and inhibit mammalian calcium-dependent Slo1 BK channels. *Nature* **425**, 531–535 (2003).
45. Zeng, F. *et al.* Human TRPC5 channel activated by a multiplicity of signals in a single cell. *J. Physiol. (Lond.)* **559**, 739–750 (2004).
46. van Rossum, D.B., Patterson, R.L., Ma, H.T. & Gill, D.L. Ca^{2+} entry mediated by store depletion, S-nitrosylation, and TRPC3 channels. *J. Biol. Chem.* **275**, 28562–28568 (2000).
47. Thyagarajan, B. *et al.* Expression of Trp3 determines sensitivity of capacitative Ca^{2+} entry to nitric oxide and mitochondrial Ca^{2+} handling: evidence for a role of Trp3 as a subunit of capacitative Ca^{2+} entry channels. *J. Biol. Chem.* **276**, 48149–48158 (2001).
48. Koliwad, S.K., Kunze, D.L. & Elliott, S.J. Oxidant stress activates a non-selective cation channel responsible for membrane depolarization in calf vascular endothelial cells. *J. Physiol. (Lond.)* **491**, 1–12 (1996).
49. Zhang, N., Beuve, A. & Townes-Anderson, E. The nitric oxide-cGMP signaling pathway differentially regulates presynaptic structural plasticity in cone and rod cells. *J. Neurosci.* **25**, 2761–2770 (2005).
50. Freichel, M. *et al.* Lack of an endothelial store-operated Ca^{2+} current impairs agonist-dependent vasorelaxation in TRP4–/– mice. *Nat. Cell Biol.* **3**, 121–127 (2001).

Available online at www.sciencedirect.com
SCIENCE DIRECT®
Phytomedicine 13 (2006) 401–411
Phytomedicine
www.elsevier.de/phymed

Screening of novel nuclear receptor agonists by a convenient reporter gene assay system using green fluorescent protein derivatives

T. Suzuki[a,b], T. Nishimaki-Mogami[a], H. Kawai[a], T. Kobayashi[a], Y. Shinozaki[a], Y. Sato[a], T. Hashimoto[c], Y. Asakawa[c], K. Inoue[a], Y. Ohno[a], T. Hayakawa[a], T. Kawanishi[a,*]

[a]*National Institute of Health Sciences, Tokyo, Japan*
[b]*Pharmaceuticals and Medical Device Agency, Tokyo, Japan*
[c]*Faculty of Pharmaceutical Sciences, Tokushima Bunri University, Tokushima, Japan*

Received 27 September 2004; accepted 6 April 2005

Abstract

Nuclear receptors represent a very good family of protein targets for the prevention and treatment of diverse diseases. In this study, we screened natural compounds and their derivatives, and discovered ligands for the retinoic acid receptors (RARs) and the farnesoid X receptor (FXR). In the reporter assay systems of nuclear receptors presented here, two fluorescent proteins, enhanced yellow fluorescent protein (EYFP) and enhanced cyan fluorescent protein (ECFP), were used for detection of a ligand-based induction and as an internal control, respectively. By optimizing the conditions (e.g., of hormone response elements and promoter genes for reporter plasmids), we established a battery of assay systems for ligands of RARs, retinoid X receptor (RXR) and FXR. The screening using the reporter assay system can be carried out without the addition of co-factors or substrates. As a result of screening of more than 140 compounds, several compounds were detected which activate RARs and/or FXR. Caffeic acid phenylethyl ester (CAPE), known as a component of propolis from honeybee hives, and other derivatives of caffeic acid up-regulated the expression of reporter gene for RARs. Grifolin and ginkgolic acids, which are non-steroidal skeleton compounds purified from mushroom or ginkgo leaves, up-regulated the expression of the reporter gene for FXR.

Keywords: FXR; RAR; Reporter assay; Fluorescence; GFP; Caffeic acid; Ginkgolic acid; Grifolin

Introduction

Nuclear hormone receptors are ligand-activated transcription factors that are involved in a variety of physiological, developmental, and toxicological processes. The nuclear hormone receptor superfamily includes receptors for thyroid and steroid hormones, retinoids and vitamin D, as well as receptors for unknown ligands. These receptors share a highly conserved DNA-binding domain and a discrete ligand-binding domain, and bind to hormone response elements (HREs) on the DNA during the formation of homodimers, heterodimers, or monomers. This ligand binding to nuclear receptors leads to conformational

*Corresponding author. Tel.: +81 3 3700 9064; fax: +81 3 3700 9084.
E-mail address: kawanish@nihs.go.jp (T. Kawanishi).

0944-7113/$ - see front matter © 2005 Elsevier GmbH. All rights reserved.
doi:10.1016/j.phymed.2005.09.003

change of these receptors and the recruitment of coactivator complexes, resulting in transcriptional activation (Khorasanizadeh and Rastinejad, 2001). Their ligand-dependent activity makes nuclear receptors good pharmacological targets.

Nuclear receptors form a superfamily of phylogenetically related proteins encoded by 48 genes in the human genome. Three isotypes of retinoic acid receptors (RARs: RARα, RARβ and RARγ) are receptors for retinoids such as all-*trans*-retinoic acid (ATRA) (Petkovich et al., 1987; Brand et al., 1988; Krust et al., 1989). RARα is associated with differentiation therapy for human acute promyelocytic leukemia (Hansen et al., 2000). RARβ plays a central role in limiting the growth of different cell types (reviewed in Hansen et al., 2000), and is thus a possible target for the treatment of breast and other cancers. RARγ is also primarily expressed in the skin and is involved in skin photoaging and carcinogenesis, and in skin diseases such as psoriasis and acne (Fisher et al., 1996).

The farnesoid X receptor (FXR) is a receptor for bile acids such as chenodeoxycholic acid (CDCA), deoxycholic acid, cholic acid, and their conjugates. Bile acids are synthesized in the liver and secreted into the intestine, where their physical properties facilitate the absorption of fats and vitamins through micelle formation. Cholesterol disposal from the liver is also dependent on the bile acid composition of the secreted bile. Bile acids bind to FXR to activate and regulate the transcription of FXR target genes. FXR controls the expression of critical genes in bile acid and cholesterol homeostasis (Makishima et al., 1999; Parks et al., 1999; Wang et al., 1999). FXR-null mice show elevated serum cholesterol and triglyceride levels (Sinal et al., 2000), and an FXR agonist has been shown to reduce serum triglyceride levels (Maloney et al., 2000). FXR is thus an attractive pharmacological target for the treatment of hyperlipidemia. Moreover, an FXR agonist has been reported to confer hepatoprotection in a rat model of cholestasis (Liu et al., 2003).

The retinoid X receptor (RXR) is a common heterodimeric partner for many receptors, including thyroid hormone receptor (TR), RAR, vitamin D_3 receptor (VDR), peroxisome proliferator-activated receptor (PPAR), liver X receptor (LXR), and FXR, in addition to functioning as a receptor for 9-*cis*-retinoic acid (9CRA) during formation of a homodimer.

To determine ligands for these nuclear receptors, we developed a reporter assay system using GFP derivatives. To study the promoter and enhancer control of gene expression, firefly luciferase is widely used as a reporter protein because it has high sensitivity and a broad linear range. In the commonly used reporter assay, β-galactosidase, a well-characterized bacterial enzyme, or renilla luciferase is usually used in conjunction with firefly luciferase to normalize the transfection efficiency of the reporter gene (Sherf et al., 1996; Martin et al., 1996). In such cases, the activity of the two reporter proteins must be measured in different ways (e.g., absorptiometry and luminescence photometry) or by using two substrates. In the reporter assay presented here, we used two species derived from green fluorescent protein (GFP), one (enhanced yellow fluorescent protein, (EYFP)) to measure the promotion and enhancement of gene expression, and the other (enhanced cyan fluorescent protein, (ECFP)) to normalize the transfection, and were thus able to measure the fluorescent protein signals simultaneously without any co-factor or substrates. As a result of screening of more than 140 compounds, it was found that several compounds activate RARs and/or FXR.

Materials and methods

Chemicals

Chenodeoxycholic acid was purchased from Sigma-Aldrich (St. Louis, MI, USA), and ATRA and 9CRA were from Wako (Osaka, Japan). Ginkgolic acid 17:1, 15:0, and 13:0 were purchased from Nagara Science (Gifu, Japan).

Purification and synthesis of test compounds

Ginkgolic acid 15:1 was purified from *Ginkgo biloba L.* var. *diptera* according to Morimoto et al. (1968). 2-Methyl ginkgolic acid methyl ester was prepared by methylation of the ginkgolic acid with methyl iodide and K_2CO_3 (Paul and Yeddanapalli, 1956; Begum et al., 2002). Grifolin was purified from *Albatrellus confluens* and *Albatrellus ovinus* (Ishii et al., 1988; Nukata et al., 2002). We isolated bazzanenyl caffeate from the liverwort *Bazzania fauriana* (Toyota and Asakawa, 1988). We synthesized caffeic acid phenethyl ester (CAPE), farnesyl caffeate and geranyl caffeate for acquirement in quantity. The synthesis of CAPE by coupling reactions of caffeic acid and β-phenylethyl bromide was reported by Hashimoto et al. (1988), and the details of the synthesis of farnesyl and geranyl caffeates are described below. The purity of the compounds for the bioactivation test was shown to be over 95% by ^1H and ^{13}C NMR spectra.

Synthesis of farnesyl caffeate

Twenty-five percent NaOH (2.5 ml) was added to a solution of caffeic acid (3,4-dihydroxycinnamic acid) (2.10 g) in HMPA (hexamethylphosphoric triamide) (150 ml), and the mixture was stirred for 1 h under N_2 at room temperature. A solution of farnesyl bromide (4.98 g) in HMPA (20 ml) was added dropwise for

10 min to the reaction mixture. The reaction mixture was stirred for 24 h at room temperature, and poured in ice cold H_2O (300 ml). The organic layer, which was extracted with Et_2O (200 ml × 2), was washed with brine (300 ml), dried ($MgSO_4$) and evaporated under reduced pressure to an oil (6.75 g). The oil was chromatographed on silica gel (200 g) with a gradient solvent system of $CHCl_3$–EtOAc, increasing the amount of 2% portions EtOAc stepwise to give 32 fractions. Farnesyl caffeate (1.435 g; Y. 43.2%) was obtained from 10% EtOAc-*n*-hexane eluate (Fr. 12-18) as a pure white powder. Caffeic acid (1.025 g; Y. 48.8%), the starting material, was recovered from 20% EtOAc-*n*-hexane eluate (Fr. 25-31).

Farnesyl caffeate: EI-MS: *m/z* 384 (M^+,5%), 315, 204, 180, 163 (100%), 135, 93, 69; HR-MS: *m/z* 384.2307, $C_{24}H_{32}O_4$ requires 384.2300; anal. calcd. for $C_{24}H_{32}O_4$: C, 74.97; H, 8.39. Found: C, 74.85; H, 8.30; FT-IR (KBr) cm^{-1}: 3480 (OH), 3301 (OH), 1678 (C=O), 1600, 1278, 1183; UV (EtOH) λ_{max} nm (log ε): 333 (4.15), 303 (4.00), 248 (3.90), 220 (4.03); ^1H NMR (acetone-d_6): δ1.56 (3H, *s*, CH_3), 1.62 (3H, *s*, CH_3), 1.65 (3H, *s*, CH_3), 1.76 (3H, *s*, CH_3), 4.68 (1H, *d*, $J \doteq 7.0$ Hz, H-1′), 5.12 (2H, *m*, H-6′ and H-10′), 5.41 (1H, *t*, $J = 7.0$ Hz, H-2′), 6.26 (1H, *d*, $J = 15.9$ Hz, H-β), 6.87 (1H, *d*, $J = 8.2$ Hz, H-5), 7.03 (1H, *dd*, $J = 1.8$, 8.2 Hz, H-6), 7.15 (1H, *d*, $J = 1.8$ Hz, H-2), 7.53 (1H, *d*, $J = 15.9$ Hz, H-α), 8.26 (1H, *br.s*, –OH), 8.49 (1H, *br.s*, –OH); ^{13}C NMR ((acetone-d_6): δ16.1 (*q*, CH_3), 16.4 (*q*, CH_3), 17.7 (*q*, CH_3), 25.8 (*q*, CH_3), 26.8 (*t*, CH_2), 27.4 (*t*, CH_2), 40.1 (*t*, CH_2), 40.4 (*t*, CH_2), 61.3 (*t*, CH_2), 115.1 (*d*, CH), 115.7 (*d*, CH), 116.3 (*d*, CH), 120.1 (*d*, CH), 122.4 (*d*, CH), 124.6 (*d*, CH), 125.1 (*d*, CH), 127.6 (*s*, C), 131.6 (*s*, C), 135.9 (*s*, C), 142.1 (*s*, C), 145.6 (*d*, CH), 146.3 (*s*, C), 148.7 (*s*, C), 167.3 (*s*, –COO)).

Synthesis of geranyl caffeate

Twenty-five percent NaOH (2.1 ml) was added to a solution of caffeic acid (2.00 g) in HMPA (150 ml), and the mixture was stirred for 1 h under N_2 at room temperature. A solution of geranyl bromide (3.10 g) in HMPA (20 ml) was added dropwise for 10 min to the reaction mixture. The reaction mixture was treated further as described above to afford geranyl caffeate (1.48 g; Y. 61.4%) as a white powder, and caffeic acid (0.56 g; Y. 28.0%).

Geranyl caffeate: EI-MS: *m/z* 316 (M^+, 10%), 247, 180, 163 (100%), 136, 69; HR-MS: *m/z* 316.1682, $C_{19}H_{24}O_4$ requires 316.1674; anal. calcd. for $C_{19}H_{24}O_4$: C, 72.12; H, 7.65. Found: C, 72.01; H, 7.68; FT-IR (KBr) cm^{-1}: 3483 (OH), 3295 (OH), 1678 (C=O), 1599, 1278, 1183; UV (EtOH) λ_{max} nm (log ε): 334 (4.16), 302 (4.05), 249 (3.93), 222 (4.01); ^1H NMR (acetone-d_6): δ1.60 (3H, *s*, CH_3), 1.66 (3H, *s*, CH_3), 1.75 (3H, *s*, CH_3), 4.68 (1H, *d*, $J = 7.0$ Hz, H-1′), 5.12 (1H, *t*, $J = 7.0$ Hz, H-6′), 5.40 (1H, *t*, $J = 7.0$ Hz, H-2′), 6.27 (1H, *d*, $J = 15.9$ Hz, H-β), 6.87 (1H, *d*, $J = 8.2$ Hz, H-5), 7.03 (1H, *dd*, $J = 2.0$, 8.2 Hz, H-6), 7.16 (1H, *d*, $J = 2.0$ Hz, H-2), 7.55 (1H, *d*, $J = 15.9$ Hz, H-α), 8.28 (1H, *br.s*, –OH), 8.50 (1H, *br.s*, –OH); ^{13}C NMR ((acetone-d_6): δ16.4 (*q*, CH_3), 17.7(*q*, CH_3), 25.8 (*q*, CH_3), 27.0 (*t*, CH_2), 40.1 (*t*, CH_2), 61.3 (*t*, CH_2), 115.1 (*d*, CH), 115.6 (*d*, CH), 116.3 (*d*, CH), 120.0 (*d*, CH), 122.4 (*d*, CH), 124.6 (*d*, CH), 127.6 (*s*, C), 132.0 (*s*, C), 142.1 (*s*, C), 145.6 (*d*, CH), 146.3 (*s*, C), 148.7 (*s*, C), 167.3 (*s*, –COO)).

Plasmid construction

Plasmids were constructed for the expression of RXRα, FXR and RARs. The ORF regions of human RXRα, human FXR, mouse RARα1, mouse RARβ2, and mouse RARγ1 (accession numbers X52773, U68233, X57528, S56660, X15848) were amplified by PCR and inserted into pcDNA3.1 (Invitrogen, Carlsbad, CA, USA), respectively. For reporter plasmids, the luciferase region of the pGL3-Control Vector (Promega, Madison, WI, USA) was replaced with the EYFP fragment of pEYFP-N1 or the ECFP fragment of pECFP-N1 (Clontech, Palo Alto, CA, USA) using *Nco*I and *Xba*I sites. Subsequently, the simian virus 40 (SV40) early promoter was cut out with *Bgl*II and *Hin*dIII, and replaced with the thymidine kinase (TK) promoter of the pRL-TK vector (Promega) or one of several other promoters (the 3′ region of the TK promoter, the cytomegalovirus (CMV) promoter, or the minimal CMV promoter and the 3′ region of the CMV promoter (201 and 265 bp)) amplified using the following PCR primers:

5′-ggagatctggccccgcccagcgtcttgtc-3′ and 5′-ggaagcttgcggcacgctgttgacgctgttaagcgggtcgctgcaggg-3′ (3′ region of the TK promoter);
5′-ccagatcttagttattaatagtaatcaattacggggtc-3′ and 5′-ccaagcttgatctgacggttcactaaaccagc-3′ (CMV promoter);
5′-ccagatcttaggcgtgtacggtgggagg-3′ and 5′-ccaagcttaggctggatcggtcccggtg-3′ (minimal CMV promoter);
5′-ccagatcttgggagtttgttttggcacc-3′ and reverse primer of CMV promoter (CMV 201); and
5′-ccagatcttcaatgggcgtggatagcgg-3′ and reverse primer of CMV promoter (CMV265).

Double-stranded oligonucleotides containing HREs (RXRE, RARE and FXRE; shown in Fig. 1B) were ligated into the upstream region of these promoters using *Mlu*I and *Bgl*II sites. The sequences of the constructed plasmids were confirmed by sequencing using an ABI PRISM 310 Genetic Analyzer (Applied Biosystems, Foster City, CA, USA).

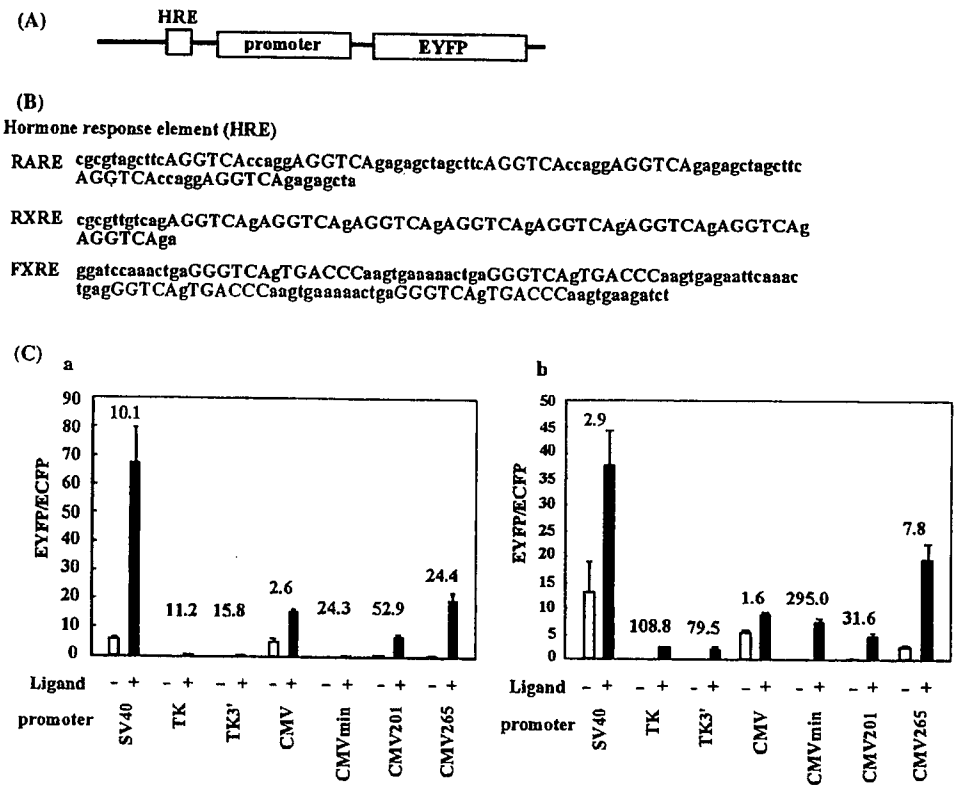

Fig. 1. Reporter plasmids for the assay of nuclear receptors. (A) Model of the constructed reporter plasmids. (B) The sequences for HREs of RAR, RXR and FXR (RARE, RXRE, and FXRE). (C) Effect of different promoters on the reporter assay. Seven species of promoter were employed in the reporter plasmid containing the HRE and EYFP genes. The activations of RARα (a) and FXR (b) are shown. The transfected cells were treated with ligands (black bar), 1 μM of ATRA for the RAR reporter assay or 100 μM of CDCA for FXR, or DMSO as a vehicle (white bar). The vertical axis indicates the ratio of fluorescence of EYFP (signal) to ECFP (internal control). The fold response relative to vehicle-treated cells is shown above the bars. Data are shown as the means + SD derived from six experiments.

Cotransfection and reporter assay

A monkey kidney cell line, COS-7, was kept in DMEM with 10% FBS. Transfections were performed using an Effectene transfection reagent (Qiagen, Valencia, CA) according to the manufacturer's instructions. The ratio of the reporter plasmid, receptor expression plasmids (for example, the RARα and RXRα expression plasmids for assay of RARα ligands) and the internal control plasmid was 4:1:1:1. The culture medium was replaced with DMEM without phenol red (Gibco BRL, Gaithersburg, MD) supplemented with 10% charcoal-treated FBS (Hyclone, Logan, UT) when the transfections were performed. At 15 h after transfections, the cells were treated with trypsin/penicillin reagent and divided among wells of a black, 96-well plate with 100 μl of the culture medium. At 6 h after division among wells, the cells were treated with chemicals. After a 40-h incubation, the medium was eliminated by decantation, the cells were washed twice with PBS, and the wells were filled with 200 μl PBS. Fluorescence was detected using a microplate reader (ARVO; Perkin Elmer, Fremont, CA, USA). The fluorescence of EYFP was detected with an excitation filter of 485 nm and an emission filter of 545 nm, and that of ECFP was detected with filters of 420 and 486 nm (Perkin Elmer), respectively. The autofluorescence in COS-7 cells was subtracted from each of the detected fluorescences, and the EYFP/ECFP ratio was calculated using the resulting values.

Results

Reporter assay system

In the present reporter assay, EYFP and ECFP were selected as a reporter protein and an internal control for normalization of transfection, respectively. These two fluorescent proteins were chosen, because the peaks of their excitation and emission wavelengths are sufficiently different (a difference of 80 and 50 nm,

respectively) so that they can be detected simultaneously without cross-detection. The considerable cross-detection between EYFP and ECFP could be prevented using a set of optical filters (see Materials and methods). The EYFP/ECFP ratio was calculated after the autofluorescence of COS-7 cells was subtracted from the fluorescence intensities of EYFP and ECFP, because the autofluorescence was not negligible.

The reporter plasmids were constructed as shown in Fig. 1A. As HREs for FXR (FXR-RXR heterodimer), RAR (RAR-RXR heterodimer) and RXR (RXR homodimer), the fragments shown in Fig. 1B were used. In order to amplify signals, we employed three copies of DR5 (direct repeat with 5 bp of spacing) and four copies of DR1 as RAR and RXR response elements (RARE and RXRE). For the FXR response element (FXRE), four copies of the response element (inverted repeat) existing in the upstream region of the phospholipid transfer protein (PLTP) gene were employed. The tandem repeats in HREs elevated the response to a sufficient degree to detect the chemicals that activated the receptor. Then, an appropriate promoter for enhancing the fluorescent signal while retaining the response to the chemicals was selected from among seven promoters (Fig. 1C). Since the SV40 or CMV promoter caused a high fluorescence intensity with or without ligands, the responses to the ligands were not strong. The response of the RAR reporter plasmid with the SV40 promoter was about ten-fold. However, the apparent rate of the response was enhanced by interference of the expression of ECFP by the expression of EYFP, because the same promoter was employed for the reporter plasmid and the internal control plasmid. Therefore, the rate did not reflect a real response, and had a large SD. The TK promoter, the 3′ region of the TK promoter and the minimal CMV promoter caused strong responses, but the expression in the control plasmid was too low for quantitative measurement. The expression of reporter proteins with the 3′ region of the CMV promoter was higher than that with TK or the minimal CMV promoter, maintaining the induction rate by the ligands. Based on a comparison between the 3′ regions of the CMV promoters, we selected the CMV201 (201 bp of the CMV promoter) promoter for use in the experiments below, since the response of CMV201 was stronger than that of CMV265.

In addition to the promoter for reporter plasmids, the promoter for the internal control plasmid and the expression plasmids of nuclear receptors were examined in order to establish an appropriate assay system of the nuclear receptor ligands. When the SV40 promoter was employed for the expression of ECFP in the internal control plasmid, the SV40 promoter for nuclear receptor expression interfered with the expression of ECFP (data not shown). Therefore, the CMV promoter was employed for nuclear receptor expression plasmids. Finally, we established the following plasmid set as the reporter assay system: a reporter plasmid containing the EYFP gene, whose expression was regulated by the HRE and CMV201 promoter; an internal control plasmid containing the ECFP gene expressed by the SV40 promoter; and the expression plasmid of the nuclear receptor containing each nuclear receptor gene expressed by the CMV promoter.

Fig. 2A shows the response to typical agonists for FXR, RARs and RXRα in the screening system. For screening of RAR ligands, three subtypes of RARs (RARα1, RARβ2, RARγ1) were expressed in the cells independently. Although endogenous RARs co-exists in the cell, the preference for the subtype of compounds could be detected. Fig. 2B and C show the dose-dependence of the assay system of FXR and RAR ligands, respectively. RARs were activated by 100 pM of ATRA. ED_{50} values were estimated to be about 1–10 nM for RARα and 0.1–1 nM for RARβ and RARγ (only the result of RARα is shown in Fig. 2B). On the other hand, activation of FXR was seen in 3–10 μM CDCA and greater activation was observed at 100 μM CDCA (Fig. 2C). These dose-dependent response patterns were comparable to those reported previously (Brand et al., 1988; Parks et al., 1999), indicating that these assays could be used for quantitative measurement of the activation by ligands. The established method of the reporter assay was described in Materials and methods.

Screening of a novel ligand for nuclear receptors

Using the established screening system, we found some natural compounds and their derivatives which acted as agonists for RARs and FXR. In the screening, there was a possibility that unexpected factors may have changed the signal responses (in the present assay system, the transcriptional efficiency may be changed irrespective of the nuclear receptor, the tested chemicals may have their own fluorescence, and so forth). Therefore, another reporter plasmid without HRE was also constructed to eliminate these unexpected factors. As this plasmid was used in place of the reporter plasmid, the compounds that regulated the expression of EYFP without HRE were eliminated. Some results of the response for each nuclear receptor are shown in Fig. 3 (RAR, upper panel; FXR, middle panel; control, lower panel). The results for RARβ are presented as representative of those for RARs. Ten millimolar of each compound referring to the stock solution in DMSO was added to the culture medium of the transfected COS-7 cells at a final concentration of 30 μM (Fig. 3, Nos. 1–26). Compound Nos. 27, 28, and 29 were 3 μM ATRA, 30 μM CDCA, and vehicle, respectively. ATRA also slightly activated the FXR-RXR heterodimer, due

to the activation of RXR. Although, for example, Nos. 16, 18, 19, and 25 enhanced the relative EYFP/ECFP ratio, these compounds also enhanced the control that was used with the reporter plasmid without HRE. Thus it was concluded that these compounds were not ligands for the nuclear receptors.

As a result of screening more than 140 compounds (a part of the results is shown in Fig. 3), five compounds were found as ligands for the nuclear receptors. CAPE (compound No. 20 in Fig. 3), geranyl caffeate (No. 21), and farnesyl caffeate (not shown in Fig. 3) were found to be RAR agonists. Ginkgolic acid 15:1 (No. 12), geranyl caffeate (No. 21), and grifolin (No. 26) were found to be FXR agonists.

The structures of the caffeic acid derivatives tested in the screening are shown in Fig. 4A. CAPE, known as an active compound of propolis from honeybee hives, was synthesized from caffeic acid and β-phenylethyl bromide and other caffeic acids were purified and synthesized as described in Materials and methods. Three of these compounds (i.e., all of those tested except for bazzanenyl caffeate) activated RARs (Fig. 4B). The cells treated with over 30 μM of these compounds were removed from wells by washing of the reporter assay, because these compounds were toxic to the cell. Therefore, the results shown are for a reporter assay conducted using lower concentrations. Although the activation of RARs could be hardly detected by a low concentration of caffeic acid-derivatives, the activation by the compounds 10–30 μM was comparable to maximum activation by ATRA. As shown in Fig. 4B, CAPE activated RARβ to a greater degree than RARα or RARγ.

As FXR agonists, geranyl caffeate, ginkgolic acid 15:1 and grifolin were found. Geranyl caffeate, the RAR agonist, highly activated FXR (Fig. 3, No. 21), but the activation of the RXR homodimer was not detected (data not shown). It could not be determined whether or not farnesyl caffeate, a compound similar to geranyl caffeate, activated FXR, because 30 μM of these compounds showed toxicity for cells. The structures of ginkgolic acids and grifolin are shown in Fig. 5A. It has been reported that ginkgolic acid 15:1 was present in ginkgolic leaves (Ahlemeyer et al., 2001), and grifolin in mushrooms (Hirata and Nakanishi, 1949; Sugiyama et al., 1992). The activations of FXR by ginkgolic acid 15:1 and geranyl caffeate were comparable to that by CDCA,

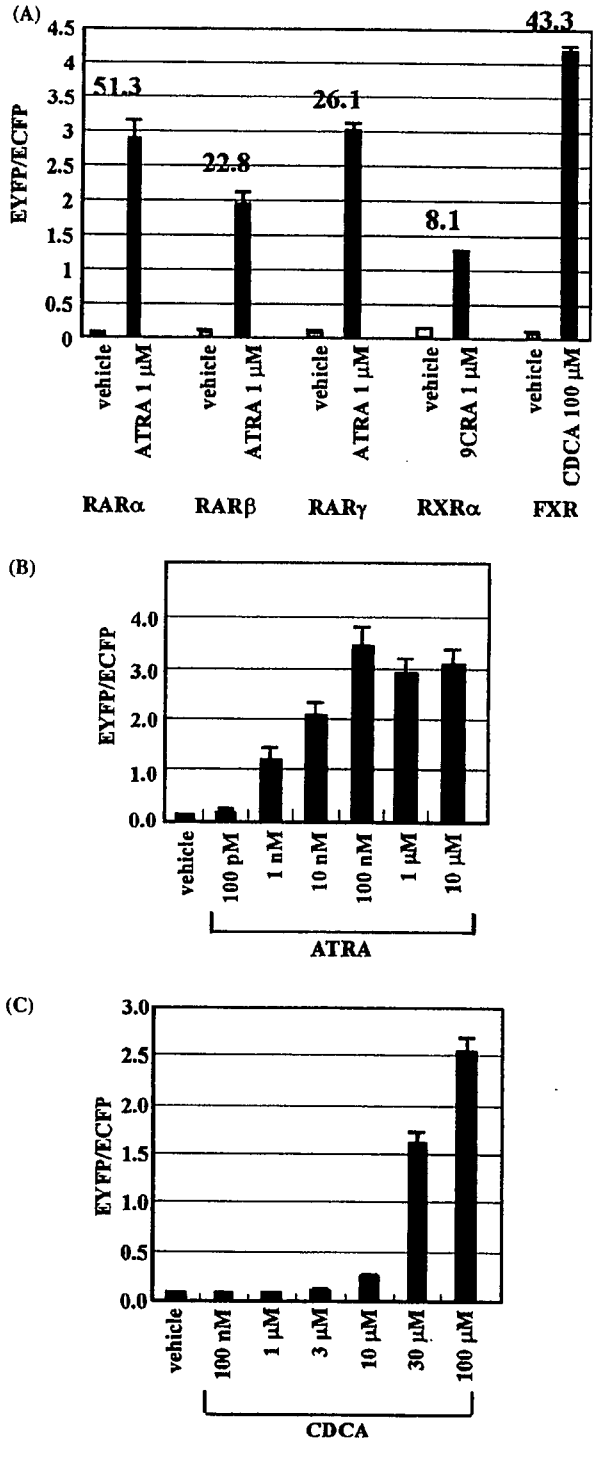

Fig. 2. Response in the reporter expression. (A) The responses in the reporter assay system by typical agonists for RAR, RXR, and FXR. COS-7 cells were transfected with an appropriate set of the plasmids (e.g. for assay of RARα ligand, the reporter plasmid containing RARE, the expression plasmids of RARα and RXRα and the internal control plasmid; for assay of RXRα ligand, the reporter plasmid containing RXRE, the RXRα expression plasmid, and the internal control plasmid). The transfected cells were treated with 1 μM of ATRA, 1 μM of 9CRA, or 100 μM of CDCA as ligands (black bar), or DMSO as a vehicle (white bar). The response rate is shown above the bars. Data are shown as the means + SD derived from three experiments. (B), (C) Dose–response analyses of ATRA and CDCA on the reporter assay of RAR and FXR. Data are shown as the means + SD derived from four experiments.

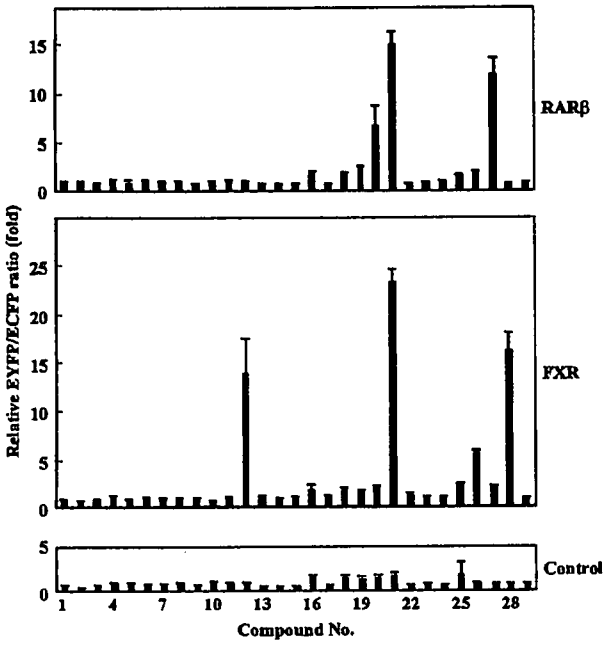

Fig. 3. Screening of ligands for RAR and FXR. COS-7 cells were transfected with the reporter plasmid, the receptor expression plasmid, and the internal control plasmid as shown in Fig. 2. The cells were treated with 30 μM of each compound. The results of the screening for RAR are shown in the upper panel, those for FXR in the middle panel, and those for the control (no HRE) in the lower panel. The results for RARβ are presented as representative of those for RARs (No. 1, hydrangeic acid; No. 2, ethyl 4′-ethylhydrangenate; No. 3, hydrangenol; No. 4, 8,3′-dimethoxyphylodulcin; No. 5, macrophyllaside A; No. 6, yashabashiletodiol A; No. 7, lycogarbin C; No. 8, lycogarbin A; No. 9, polygodial; No. 10, sacculatal; No. 11, ptychantin A; No. 12, ginkgolic acid 15:1; No. 13, 2-methyl ginkgolic acid methyl ester; No. 14, bilobal dimethyl ether; No. 15, 3-tridecanyl-*m*-cresol; No. 16, [11]-cytochalasa-6(12),13-diene-1,21-dione-7,18-dihydroxy-16,18-dimethyl-19-methoxy-10-phenyl-(7*S**,13*E*,16*S**,18*S**,19*R**); No. 17, hispidin; No. 18, costunolide, No. 19, beta-cyclocostanolide; No. 20, caffeic acid phenethyl ester; No. 21, geranyl caffeate; No. 22, atroctylon).

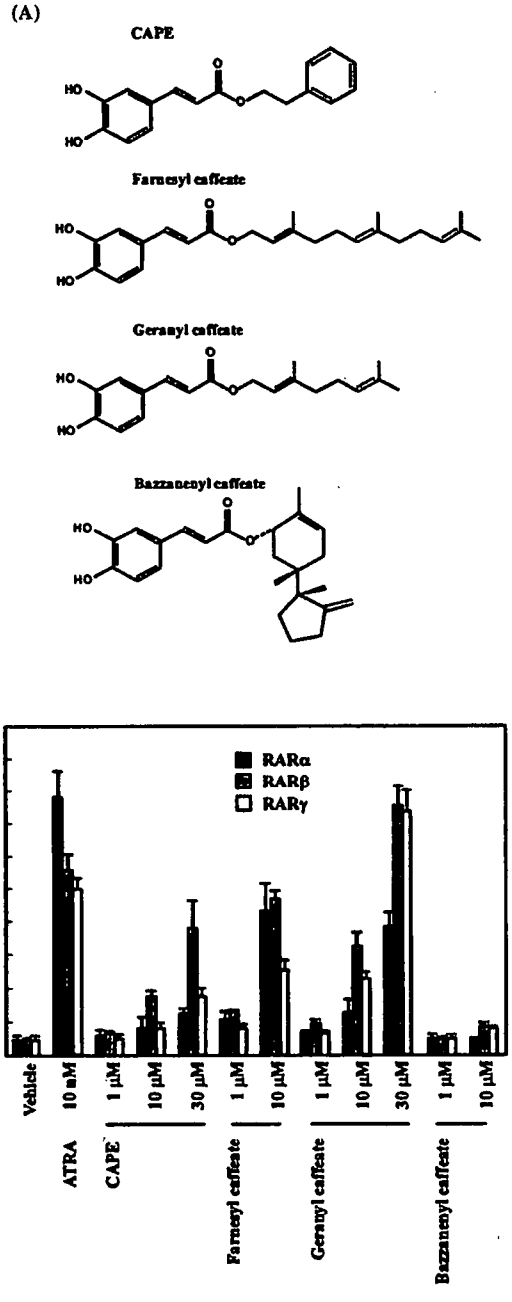

Fig. 4. Ligands for RARs. (A) The structures of caffeic acid derivatives tested in the screening. (B) Response in the RAR reporter assay. The responses in the COS-7 cells expressing RARα, RARβ or RARγ are indicated by black, gray, and white bars, respectively. Data are expressed as the fold response relative to vehicle (0.1% DMSO)-treated cells and are shown as the means + SD derived from four experiments.

the most potent endogenous bile acid. Ginkgolic acids 17:1, 15:0 and 13:0 (described in Fig. 5A) were also investigated as the other ginkgolic acids of ginkgo leaves (Fig. 5B). Ginkgolic acid 17:1 activated FXR more strongly than did 15:1, and ginkgolic acids with an alkyl chain (13:0, 15:0) activated FXR at concentrations of more than 20 μM. It seemed that the double bond and length of the carbon chain had an influence on FXR activation. Moreover, the structures except for the carbon chain were also important for FXR activation, because the methylated compound of ginkgolic acid 15:1 (2-methyl ginkgolic acid methyl ester, Fig. 5A) had no potency for FXR activation (Fig. 3, No. 13).

Discussion

To discover ligands for the nuclear receptors, we developed a battery of reporter assay systems

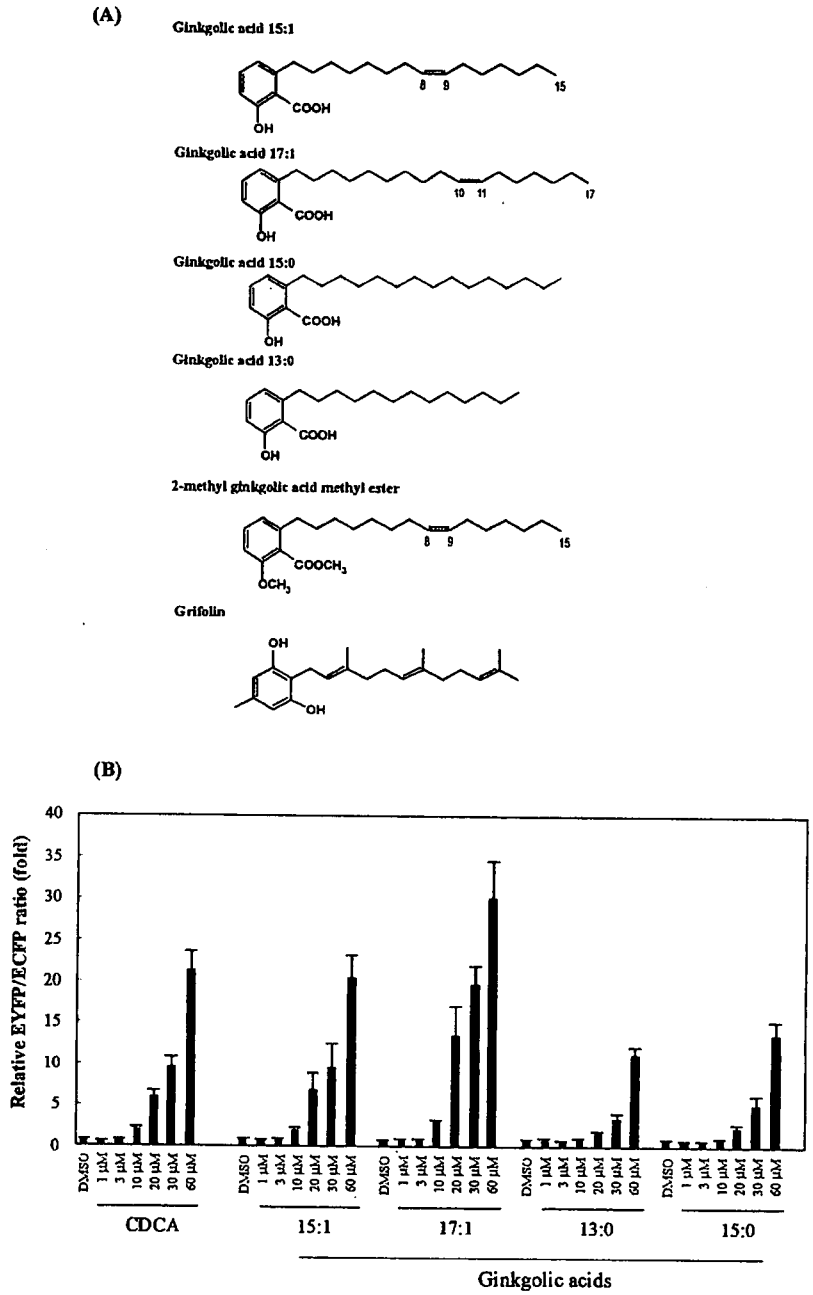

Fig. 5. Ligands for FXR. (A) The structure of candidates for FXR agonists and their related compounds (2-methyl ginkgolic acid methyl ester). (B) The activation of FXR by ginkgolic acids. COS-7 cells were transfected with the reporter plasmid containing FXRE, the expression plasmids of FXR and RXRα and the internal control plasmid. The transfected cells were treated with each compound. Data are shown as the means + SD derived from four experiments.

incorporating the advantages of fluorescent proteins. The disadvantage of GFP (low sensitivity) could be overcome by modifications. The present screening system using fluorescent proteins has clear merits of a high efficiency, convenience and low cost, because the two fluorescent signals can be measured simultaneously without addition of any co-factors. Moreover, the fluorescent signal was stable for more than 2 h after the wash. Considering these merits, this reporter assay system with fluorescent proteins might be advantageous for automatic high-throughput screening. If the expression of the fluorescent protein can be increased, the measurement of fluorescence can be carried out in culture medium, and the signal can be measured by time-course without any treatment. Moreover, the use of three fluorescent proteins (for example, DsRed with EYFP and ECFP) would enable us to carry out more efficient measurement.

Using this assay system, several compounds that induce expression of the reporter gene for RARs and/or FXR were identified. These compounds were described as ligands in this report, although there is a possibility that these compounds are metabolized and their metabolites bind to the receptors as ligands.

Three new ligands for RARs were identified: CAPE, geranyl caffeate, and farnesyl caffeate. The whole structure of these compounds may be needed for RAR-activation, because caffeic acid, a constituent compound of the compounds, did not activate RARs (data not shown). CAPE has been reported to have antioxidant, antiviral, anti-inflammatory and immunomodulatory activities (Grunberger et al., 1988), and has also been shown to inhibit the growth of different types of oncogene-transformed cells and to induce apoptosis (Grunberger et al., 1988; Burke et al., 1995; Su et al., 1994; Watabe et al., 2004). Since RARs have been reported to mediate many biological processes, it is possible that some of the diverse activities are due to their binding to RARs. Since geranyl and farnesyl caffeate have also been reported to exert antioxidant effects and to inhibit the growth of cancer cells (Inoue et al., 2004), the three compounds may suppress the growth of cancer by at least two pathways: induction of RAR and antioxidant effects. Considering its preferential activation of RARβ (Fig. 4B), CAPE may inhibit cancer (e.g., lung cancer) growth more selectively without substantial toxicity, such as the triglyceride elevation associated with RARα, and the skin, bone and teratogenic toxicity associated with RARγ Thus, especially CAPE could be assumed to be a seed for the development of an anti-cancer drug.

We also found that two natural compounds, ginkgolic acids and grifolin, activated FXR. Grifolin was first isolated as an antibiotic constituent of a mushroom, *Grifola confluens* (Hirata and Nakanishi, 1949). In 1992, it was reported that grifolin decreased liver cholesterol content, plasma total cholesterol levels, and plasma (very low-density lipoprotein (VLDL) + low-density lipoprotein (LDL)) cholesterol levels, and increased plasma high-density lipoprotein (HDL) cholesterol and plasma triglyceride levels (Sugiyama et al., 1992). It has been suggested that the effect of grifolin might be elicited, at least in part, by the augmented excretion of cholesterol into the faces (Sugiyama et al., 1994). On the other hand, FXR controls the expression of critical genes in bile acid and cholesterol homeostasis. In fact, FXR-null mice show elevated serum cholesterol and triglyceride levels (Sinal et al., 2000), and an FXR agonist has been shown to reduce serum triglyceride levels (Maloney et al., 2000). Moreover, FXR induces the expression of the gene of PLTP, which plays a role in HDL metabolism (Urizar et al., 2000). It seems that the cholesterol-lowering and HDL-cholesterol-increasing effects of grifolin are related to FXR activation, although grifolin's enhancement of triglyceride production was not consistent with its down-regulation of FXR agonists.

The FXR agonists found in this study are all non-steroidal compounds, whereas the well-known ligand of FXR, bile acid, is a steroidal one. The common characteristic of the structure of the ligands is their long carbon chains (i.e., geranyl, farnesyl and pentadecenyl), and farnesol has been shown to be a FXR ligand (Forman et al., 1995). However, aspects of the structures other than the carbon chains also appear to be important for FXR activation, because geraniol, a constituent compound of geranyl caffeate, has been reported not to activate FXR (Forman et al., 1995), and the methylated compound of ginkgolic acid 15:1 had no potency for FXR activation in the present study.

Several compounds, such as TTNPB, GW4064, Farnesoid, Forskolin, Fexaramine, AGN29 and AGN31, have been reported as non-steroidal agonists (Maloney et al., 2000; Howard et al., 2000; Downes et al., 2003; Dussault et al., 2003). The non-steroidal ligands may be important tools for studying the pharmacology of the receptor, because they may not have the property of bile acids and are not metabolized to form harmful lithocholic acid (Fischer et al., 1996; Javitt, 1966). In the present study, ginkgolic acids and geranyl caffeate strongly activated FXR, and both had structures quite different from bile acids, so that they could be good tools in this sense. Moreover, the importance of identifying gene-selective modulators that regulate a subset of FXR-specific genes as therapeutic agents has been recognized (Cui et al., 2003; Dussault et al., 2003). The gene-selective modulators of estrogen receptor, selective estrogen receptor modulators (SERMs), have been well studied (reviewed in McDonnell et al., 2002), and some compounds with a structure divergent from that of estrogen have been identified and applied to therapies of breast cancer and osteoporosis. The non-steroidal compounds could also be good tools for studying the selective response of FXR target genes.

In this report, we developed a new method for screening novel nuclear receptor agonists, and used it to identify new candidate ligands for FXR and RARs. We expect that these new ligands will be good pharmacological tools. Since the compound whose structure is much different from bile acids is expected to possess a specific effect as a ligand, we continue to screen various ligands from natural compounds with a wide variety of structures.

Acknowledgements

This work was supported by a grant-in-aid (MF-16) from the Pharmaceuticals and Medical Device Agency, a grant-in-aid for Research on Health Sciences Focusing

on Drug Innovation from the Japan Health Science Foundation, and a grant-in-aid for Research on Advanced Medical Technology from the Ministry of Health, Labour and Welfare of Japan.

References

Ahlemeyer, B., Selke, D., Schaper, C., Klumpp, S., Krieglstein, J., 2001. Ginkgolic acids induce neuronal death and activate protein phosphatase type-2C. Eur. J. Pharmacol. 430, 1–7.

Begum, P., Hashidoko, Y., Islam, M.T., Ogawa, Y., Tahara, S., 2002. Zoosporicidal activities of anacardic acids against *Aphanomyces cochlioides*. Z. Naturforsch. [C] 57, 874–882.

Brand, N., Petkovich, M., Krust, A., Chambon, P., de Thé, H., Marchio, A., Tiollais, P., Dejean, A., 1988. Identification of a second human retinoic acid receptor. Nature 332, 850–853.

Burke Jr., T.R., Fesen, M.R., Mazumder, A., Wang, J., Carothers, A.M., Grunberger, D., Driscoll, J., Kohn, K., Pommier, Y., 1995. Hydroxylated aromatic inhibitors of HIV-1 intergrase. J. Med. Chem. 38, 4171–4178.

Cui, J., Huang, L., Zhao, A., Lew, J.-L., Yu, J., Sahoo, S., Meinke, P.T., Royo, I., Peláez, F., Wright, S.D., 2003. Guggulsterone is a farnesoid X receptor antagonist in coactivator association assays but acts to enhance transcription of bile salt export pump. J. Biol. Chem. 278, 10214–10220.

Downes, M., Verdecia, M.A., Roecker, A.J., Hughes, R., Hogenesch, J.B., Kast-Woelbern, H.R., Bowman, M.E., Ferrer, J.-L., Anisfeld, A.M., Edwards, P.A., Rosenfeld, J.M., Alvarez, J.G.A., Noel, J.P., Nicolaou, K.C., Evans, R.M., 2003. A chemical, genetic, and structural analysis of the nuclear bile acid receptor FXR. Mol. Cell 11, 1079–1092.

Dussault, I., Beard, R., Lin, M., Hollister, K., Chen, J., Xiao, J.H., Chandraratna, R., Forman, B.M., 2003. Identification of gene-selective modulators of the bile acid receptor FXR. J. Biol. Chem. 278, 7027–7033.

Fischer, S., Beuers, U., Spengler, U., Zwiebel, F.M., Koebe, H.G., 1996. Hepatic levels of bile acids in end-stage chronic cholestatic liver disease. Clin. Chim. Acta 251, 173–186.

Fisher, G.J., Voorhees, J.J., 1996. Molecular mechanisms of retinoid actions in skin. FASEB J. 10, 1002–1013.

Forman, B.M., Goode, E., Chen, J., Oro, A.E., Bradley, D.J., Perlmann, T., Noonan, D.J., Burka, L.T., McMorris, T., Lamph, W.W., Evans, R.M., Weinberger, C., 1995. Identification of a nuclear receptor that is activated by farnesol metabolites. Cell 81, 687–693.

Grunberger, D., Banerjee, R., Eisinger, K., Oltz, E.M., Efros, L., Caldwell, M., Estevez, V., Nakanishi, K., 1988. Preferential cytotoxity on tumor cells by caffeic acid phenethyl ester isolated from propolis. Experientia 44, 230–232.

Hansen, L.A., Sigman, C.C., Andreola, F., Ross, S.A., Kelloff, G.J., De Luca, L.M., 2000. Retinoids in chemoprevention and differentiation therapy. Carcinogenesis 21, 1271–1279.

Hashimoto, T., Tori, M., Asakawa, Y., Wollenweber, E., 1988. Synthesis of two allergenic constituents of propolis and poplar bud excretion. Z. Naturforsch. [C] 43, 470–472.

Hirata, Y., Nakanishi, K., 1949. Grifolin, an antibiotic from a basidiomycete. J. Biol. Chem. 184, 135–143.

Howard, W.R., Pospisil, J.A., Njolito, E., Noonan, D.J., 2000. Catabolites of cholesterol synthesis pathways and forskolin as activators of the farnesoid X-activated nuclear receptor. Toxicol. Appl. Pharmacol. 163, 195–202.

Inoue, K., Nishitani, N., Tanabe, A., Yamanaka, H., Hashimoto, T., Asakawa, Y., Fujiki, H., 2004. Significance of structural specificity in the antioxidant activity of hydrangenol and caffeic acid-derivatives. Abstract for 124th Congress on Nihon yakugakukai, Osaka, Japan, vol. 2, p. 173.

Ishii, N., Takahashi, A., Kusano, G., Nozoe, S., 1988. Studies on the constituents of *Polyporus dispansus* and *P. confluens*. Chem. Pharm. Bull. 36, 2918–2924.

Javitt, N.B., 1966. Cholestasis in rats induced by taurolithocholate. Nature 210, 1262–1263.

Khorasanizadeh, S., Rastinejad, F., 2001. Nuclear-receptor interactions on DNA-response elements. Trends Biochem. Sci. 26, 384–390.

Krust, A., Kastner, P.H., Petkovich, M., Zelent, A., Chambon, P., 1989. A third human retinoic acid receptor, hRAR-γ. Proc. Natl. Acad. Sci. USA 86, 5310–5314.

Liu, Y., Binz, J., Numerick, M.J., Dennis, S., Luo, G., Desai, B., MacKenzie, K.I., Mansfield, T.A., Kliewer, S.A., Goodwin, B., Jones, S.A., 2003. Hepatoprotection by the farnesoid X receptor agonist GW4064 in rat models of intra- and extrahepatic cholestasis. J. Clin. Invest. 112, 1678–1687.

Makishima, M., Okamoto, A.Y., Repa, J.J., Tu, H., Learned, R.M., Luk, A., Hull, M.V., Lustig, K.D., Mangelsdorf, D.J., Shan, B., 1999. Identification of a nuclear receptor for bile acids. Science 284, 1362–1365.

Maloney, P.R., Parks, D.J., Haffner, C.D., Fivush, A.M., Chandra, G., Plunket, K.D., Creech, K.L., Moore, L.B., Wilson, J.G., Lewis, M.C., Jones, S.A., Willson, T.M., 2000. Identification of a chemical tool for the orphan nuclear receptor FXR. J. Med. Chem. 43, 2971–2974.

Martin, C.S., Wight, P.A., Dobretsova, A., Bronstein, I., 1996. Dual luminescence-based reporter gene assay for luciferase and β-galactosidase. Biotechniques 21, 520–524.

McDonnell, D.P., Connor, C.E., Wijayaratne, A., Chang, C.Y., Norris, J.D., 2002. Definition of the molecular and cellular mechanisms underlying the tissue-selective agonist/antagonist activities of selective estrogen receptor modulators. Recent Prog. Horm. Res. 57, 295–316.

Morimoto, H., Kawamatsu, Y., Sugihara, H., 1968. Stereostructure of toxin from the fruit of *Ginkgo biloba L.* Chem. Pharm. Bull. 16, 2282–2286.

Nukata, M., Hashimoto, T., Yamamoto, I., Iwasaki, N., Tanaka, M., Asakawa, Y., 2002. Neogrifolin derivatives possessing anti-oxidative activity from the mushroom *Albatrellus ovinus*. Phytochemistry 59, 731–737.

Parks, D.J., Blanchard, S.G., Bledsoe, R.K., Chandra, G., Consler, T.G., Kliewer, S.A., Stimmel, J.B., Willson, T.M., Zavacki, A.M., Moore, D.D., Lehmann, J.M., 1999. Bile acids: natural ligands for an orphan nuclear receptor. Science 284, 1365–1368.